

Supporting Information

For

Alkyne hydrazones for Raman scattering spectroscopy

Daniil Sosnin, and Ivan Aprahamian*

6128 Burke Laboratory, Department of Chemistry, Dartmouth College, Hanover, New
Hampshire 03755, United States
Email: ivan.aprahamian@dartmouth.edu

Table of Contents

1. General Methods	3
2. Synthesis	5
3. NMR Spectroscopy Characterization	9
4. Photoisomerization Studies	20
5. Photostationary States Studies	23
6. Photoisomerization Quantum Yield Measurements	29
7. Raman Scattering Spectroscopy Studies	42
8. Kinetic Studies	48
9. Single Crystal Diffraction Studies	54
10. References	60

1. General Methods

Materials and Methods:

All reagents and starting materials were purchased from commercial vendors and used as supplied unless otherwise indicated. All experiments were conducted under air unless otherwise noted. Compounds were purified by column chromatography using silica gel (SiliCycle[®], 60 Å, 230-400 mesh) as stationary phase and solvents mixtures used during chromatography were reported as volume ratios unless otherwise noted. Deuterated solvents were purchased from Cambridge Isotope Laboratories, Inc. and used as received. ¹H NMR, ¹³C NMR and 2D NMR spectra were recorded on a 500 or 600 MHz NMR spectrometer, with working frequencies of 500.13 or 600.13 MHz for ¹H nuclei, and 125.8 or 150.9 MHz for ¹³C nuclei, respectively. Chemical shifts are quoted in ppm relative to tetramethylsilane (TMS), using the residual solvent peak as the reference standard. ESI mass spectra were obtained on a Waters Quattro II ESI mass spectrometer. Melting points were measured on an Electrothermal Thermo Scientific IA9100X1 digital melting point instrument. UV-Vis spectra were recorded on a Shimadzu UV-1800 UV-Vis spectrophotometer.

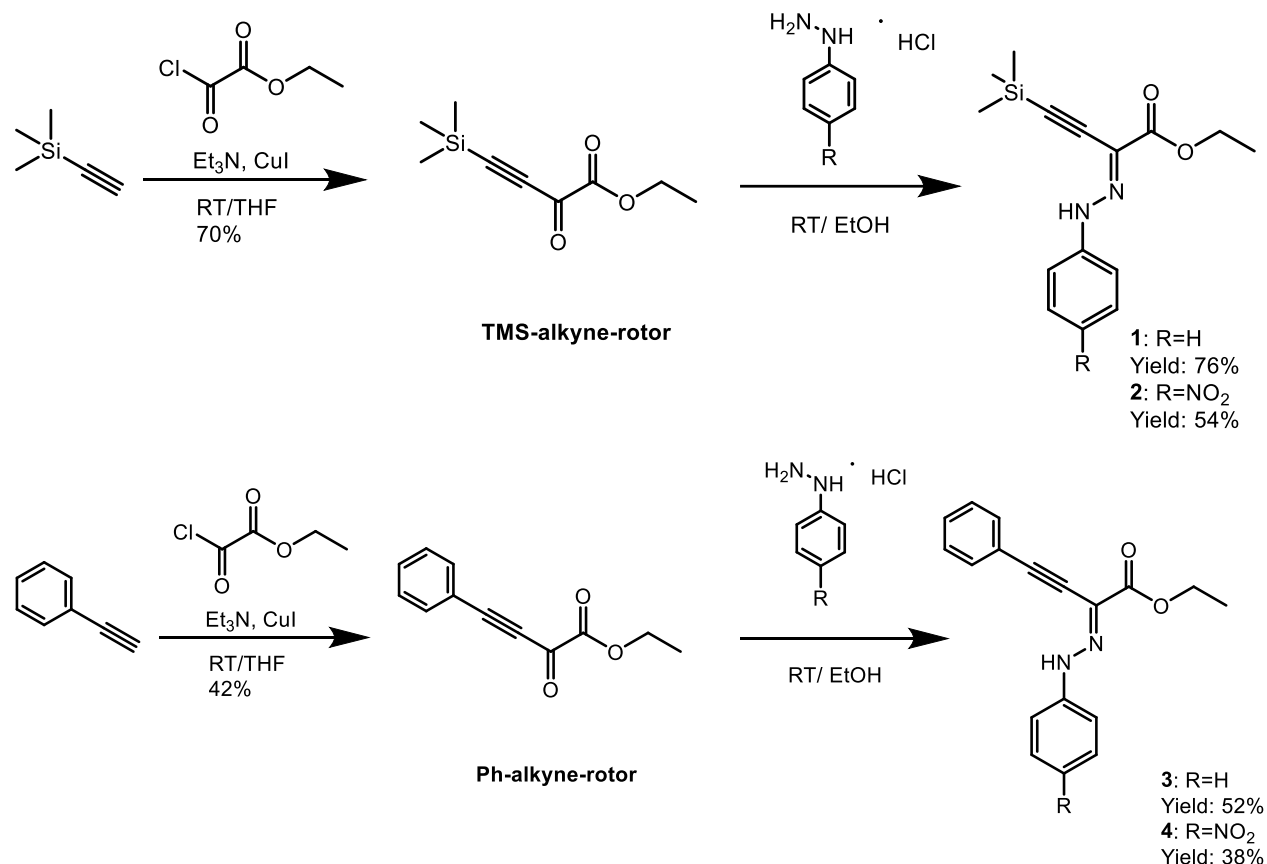
Irradiation experiments were conducted with a stand-alone xenon arc lamp system (Model: LB-LS/30, Sutter Instrument Co.), outfitted with a SMART SHUTTER controller (Model: LB10-B/IQ, Sutter Instrument Co.) and a liquid light guide LLG/250. 340 (part number: 340HC10-25), 410 (part number: 410FS10-25), 442 (part number: 442F5X10-25), and 480 (part number: 480HC10-25) nm light filters, purchased from Andover Corporation, were used in the irradiation experiments.

Raman Spectroscopy experiments were carried out on a Horiba Scientific LabRAM HR Evolution Raman spectrometer using a liquid cell holder for 1 cm standard cuvettes. For excitation 532 and 633 nm wavelength lasers were used. For each measurement a fresh solution of hydrazone was prepared (1×10^{-3} M) in spectroscopic grade toluene, and 2 ml was then transferred into the 1 cm standard quartz cuvette. Following each measurement the samples were irradiated with an appropriate wavelength to induce isomerization, and the afforded spectra were collected. All measurements were done in triplicates and under dark to minimize photoisomerization from ambient light. Acquisition and accumulation parameters were optimized for each molecule.

2. Synthesis

2.1 Synthesis of Alkyne Hydrazones.

Scheme S1. Summary of the synthetic pathway used to access hydrazone **1-4**.



TMS-alkyne-rotor: This compound was synthesized using a reported procedure.^{S1} Briefly, CuI (49 mg, 0.25 mmol, 0.050 eq.), triethylamine (1.4 mL, 10 mmol, 2.0 eq), and THF (20 mL) were added to round bottom flask and stirred at room temperature. Once a colorless, clear solution formed, the trimethylsilylacetylene (0.50 g, 5.1 mmol, 1.0 eq.) and ethyl chlorooxoacetate (1.1 mL, 10 mmol, 2.0 eq.) were added, and the reaction was allowed to proceed at room temperature. After the reaction was done, 30 mL of water was added to the solution and extracted with DCM. The combined organic phases were dried over Na₂SO₄ and concentrated under reduced pressure. The obtained product was subsequently purified using column chromatography (0-12% ethyl acetate to hexanes). The title compound was obtained as a brown oil (0.70 g, 70% yield) and its identity was confirmed by comparing the obtained ¹H NMR spectrum with the published one. ¹H NMR (600 MHz, CDCl₃) δ 7.60 (d, *J* = 8.2 Hz, 2H), 7.46 (t, *J* = 7.4 Hz, 1H), 7.36 (t, *J* = 7.7 Hz, 2H), 4.31 (q, *J* = 7.1 Hz, 2H), 1.33 (t, *J* = 7.1 Hz, 3H) ppm.

Ph-alkyne-rotor: The title compound was obtained following the same synthetic protocol as **TMS-alkyne-rotor** using phenylacetylene as starting substrate and its identity was confirmed by comparing the obtained ^1H NMR spectrum with the published one.^{S2} ^1H NMR (600 MHz, CDCl_3) δ 4.17 (q, $J = 7.1$ Hz, 5H), 1.21 (d, $J = 7.3$ Hz, 3H), 0.10 (s, 9H) ppm.

General Synthetic Procedure for the Hydrazone Molecules:

α -Ketoester rotor **1** or **2** (0.10 g, 0.45 mmol, 1 eq) and phenylhydrazine (0.91 mmol, 2 eq) were dissolved in 10 mL of EtOH and stirred at room temperature. After the reaction was done a large amount of water was added to the solution and the product was extracted with DCM. The combined organic layers were dried over sodium sulphate and concentrated under reduced pressure. The product was purified by column chromatography (0-5% EtAc:Hex).

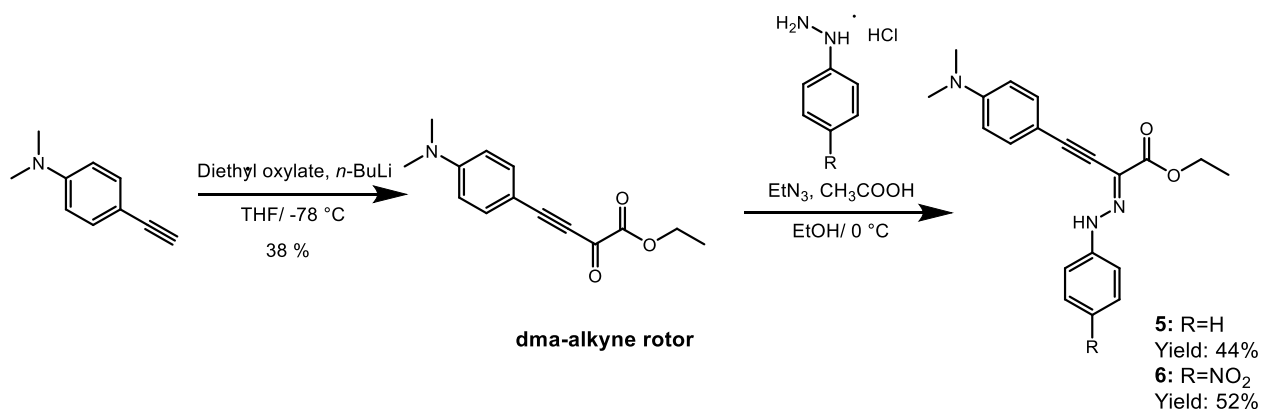
1: The title compound was obtained as brown solid in 76% yield. m.p. 70.7-71.5 °C; ^1H NMR (600 MHz, CD_2Cl_2) δ 9.03 (s, 1H), 7.29 (t, $J = 15.7$ Hz, 2H), 7.17 (t, $J = 1.1$ Hz, 2H), 7.01 (t, $J = 1.1$ Hz, 1H), 4.25 (q, $J = 0.7$ Hz, 2H), 1.30 (t, $J = 0.8$ Hz, 3H), 0.28 (s, 9H) ppm. ^{13}C NMR (151 MHz, CD_2Cl_2) δ 163.88, 143.25, 130.94, 124.83, 118.96, 116.10, 114.00, 94.02, 62.83, 15.52 ppm. Hi-Res ESI-MS: m/z found $[\text{M}-\text{H}^+]$ for $\text{C}_{15}\text{H}_{21}\text{N}_2\text{O}_2\text{Si}^+$ 289.1361 (calcd. 289.1372).

2: The title compound was obtained as yellow solid in 54% yield. m.p. 112.7-113.6 °C; ^1H NMR (600 MHz, CD_2Cl_2) δ 9.25 (s, 1H), 8.27 (d, $J = 9.3$ Hz, 2H), 7.36 (d, $J = 8.9$ Hz, 2H), 4.37 (q, $J = 7.1$ Hz, 2H), 1.41 (t, $J = 7.1$ Hz, 3H), 0.39 (s, 9H) ppm. ^{13}C NMR (151 MHz, CD_2Cl_2) δ 163.23, 148.49, 144.49, 127.37, 123.19, 115.83, 115.69, 93.34, 63.48, 15.57 ppm. Hi-Res ESI-MS: m/z found $[\text{M}-\text{H}^+]$ for $\text{C}_{15}\text{H}_{20}\text{N}_3\text{O}_4\text{Si}^+$ 334.1221 (calcd. 334.1223).

3: The title compound was obtained as yellowish solid in 52% yield. m.p. 80.5-81.0 °C; ^1H NMR (600 MHz, CD_2Cl_2) δ 9.05 (s, 1H), 7.56 – 7.51 (m, 2H), 7.41 – 7.33 (m, 3H), 7.28 (t, $J = 7.2$ Hz, 2H), 7.20 (d, $J = 8.3$ Hz, 2H), 6.99 (t, $J = 1.2$ Hz, 1H), 4.27 (q, $J = 7.1$ Hz, 2H), 1.31 (t, $J = 7.1$ Hz, 3H) ppm. ^{13}C NMR (151 MHz, CD_2Cl_2) δ 162.61, 141.98, 131.85, 129.77, 129.48, 128.67, 123.27, 121.25, 117.57, 114.65, 104.60, 77.66, 61.48, 14.13 ppm. Hi-Res ESI-MS: m/z found $[\text{M}-\text{H}^+]$ for $\text{C}_{18}\text{H}_{17}\text{N}_5\text{O}_2^+$ 293.1288 (calcd. 293.1290).

4 The title compound was obtained as yellow solid in 38% yield. m.p. 152.6-153.4 °C; ¹H NMR (600 MHz, CD₂Cl₂) δ 9.19 (s, 1H), 8.16 (d, *J* = 9.4 Hz, 2H), 7.56 (d, *J* = 7.4 Hz, 2H), 7.42 (dd, *J* = 8.4, 5.9 Hz, 1H), 7.38 (t, *J* = 7.5 Hz, 2H), 7.30 (d, *J* = 8.7 Hz, 2H), 4.30 (q, *J* = 7.2 Hz, 2H), 1.32 (t, *J* = 7.2 Hz, 3H) ppm. ¹³C NMR (151 MHz, CD₂Cl₂) δ 161.84, 147.08, 142.83, 132.02, 130.30, 128.77, 125.79, 121.74, 120.62, 114.21, 105.63, 77.11, 62.00, 14.05 ppm. Hi-Res ESI-MS: *m/z* found [M-H⁺] for C₁₈H₁₆N₃O₄⁺ 338.1135 (calcd. 338.1141).

Scheme S2. Summary of the synthetic pathway used to access hydrazones **5** and **6**



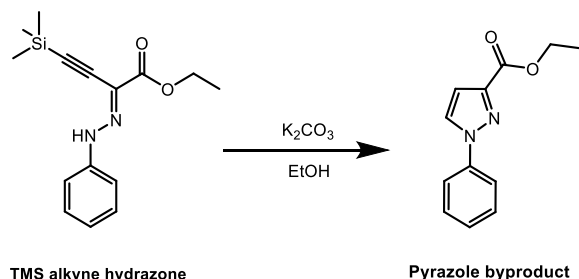
DMA-alkyne-rotor: 4-Dimethylaminophenyl acetylene (1.0 g, 6.9 mmol, 1 eq.) in THF (10 ml) was added to a flame-dried flask and the solution was cooled to -78 °C. 2.5 M *n*-BuLi in hexanes (4.1 ml, 10.3 mmol, 1.5 eq.) was then added dropwise to the solution, which was left to stir for 30 min at low temperature. Diethyl oxalate (1.4 ml, 10.3 mmol, 1.5 eq.) dissolved in THF (5 ml) was then added dropwise to the lithium reagent, and the solution was stirred for 3 hours at low temperature. The mixture was then left to warm up to room temperature and stirred for another 3 hours, after which it was quenched with a brine solution. The mixture was then extracted with CH₂Cl₂ (50 ml × 3). The organic layer was separated and dried over Na₂SO₄. After removal of the solvent under reduced pressure, the crude product was subjected to column chromatography (0-8 % EtAc:Hex). The title compound was obtained as a red solid (0.6 g, 38% yield). m.p. 62.4-62.8 °C; ¹H NMR (600 MHz, CDCl₃) δ 7.48 (d, *J* = 8.9 Hz, 2H), 6.57 (d, *J* = 9.2 Hz, 2H), 4.32 (q, *J* = 7.1 Hz, 2H), 3.00 (s, 5H), 1.35 (t, *J* = 7.1 Hz, 3H) ppm. ¹³C NMR (151 MHz, CDCl₃) δ 168.79, 160.02,

152.50, 136.31, 111.57, 104.27, 89.99, 62.97, 40.02, 14.06 ppm. ESI-MS: m/z found $[M-H]^+$ for $C_{14}H_{16}NO_3^+$ 246.15 (calcd. 246.11).

5: Phenyl hydrazine hydrochloride (0.089 g, 0.61 mmol, 1.5 eq.) and triethylamine (0.086 ml, 0.61 mmol, 1.5 eq.) were dissolved in cooled EtOH (2 ml) at 0 °C. Compound **3** (0.1 g, 0.41 mmol, 1 eq.) was dissolved in EtOH (2 ml) and added to the stirred phenylhydrazine solution at 0 °C. After 1 h a few drops of acetic acid were added to the reaction. The reaction was stopped after 4 hs and the precipitate was filtered and recrystallized using DCM : Hexane (1 : 1) solvent mixture. The title compound was obtained as a yellow solid (60 mg, 44% yield). m.p. 122.2-123.0 °C 1H NMR (600 MHz, CD_2Cl_2) δ 8.99 (s, 1H), 7.38 (d, $J = 9.0$ Hz, 2H), 7.26 (d, $J = 8.5$ Hz, 2H), 7.18 (d, $J = 7.4$ Hz, 2H), 6.95 (t, $J = 7.4$ Hz, 1H), 6.62 (d, $J = 8.9$ Hz, 2H), 4.26 (q, $J = 7.1$ Hz, 2H), 2.94 (s, 5H), 1.31 (t, $J = 7.1$ Hz, 3H) ppm. ^{13}C NMR (151 MHz, CD_2Cl_2) δ 162.83, 151.07, 142.24, 133.10, 129.43, 122.79, 118.61, 114.42, 111.60, 106.96, 106.93, 76.40, 61.38, 53.81, 53.63, 53.45, 53.27, 53.09, 39.86, 14.15 ppm. Hi-Res ESI-MS: m/z found $[M-H]^+$ for $C_{20}H_{22}N_3O_2^+$ 336.1715 (calcd. 336.1712).

6: The title compound was obtained following the same synthetic protocol used for **5** starting from 4-nitrophenyl hydrazine hydrochloride. The title compound was obtained as a red solid in 52% yield. m.p. 175.5-176.0 °C 1H NMR (600 MHz, CD_2Cl_2) δ 9.15 (s, 1H), 8.13 (d, $J = 8.7$ Hz, 2H), 7.38 (d, $J = 8.4$ Hz, 2H), 7.25 (d, $J = 8.7$ Hz, 2H), 6.61 (d, $J = 8.4$ Hz, 2H), 4.28 (q, $J = 7.1$ Hz, 2H), 2.95 (s, 5H), 1.31 (t, $J = 7.1$ Hz, 3H) ppm. ^{13}C NMR (151 MHz, CD_2Cl_2) δ 162.13, 151.37, 147.41, 142.39, 133.39, 125.80, 122.88, 113.91, 111.58, 108.51, 106.09, 76.38, 61.88, 53.82, 53.64, 53.46, 53.28, 53.10, 39.83, 14.07 ppm. Hi-Res ESI-MS: m/z found $[M-H]^+$ for $C_{20}H_{21}N_4O_4^+$ 381.1556 (calcd. 381.1563).

Scheme S4. The intramolecular cyclization to form the pyrazole byproduct.



Pyrazole byproduct: TMS alkyne hydrazone (0.10 g, 0.45 mmol, 1 eq) and K_2CO_3 (0.15 g, 1.02 mmol, 3 eq) were added to a round bottom flask and dissolved with 5 mL EtOH. The mixture was then stirred at room temperature for 10 min, and the reaction was monitored using thin layer chromatography, which revealed the generation of a new product. The mixture was quenched with a 5% HCl solution and then extracted with DCM. The combined organic phases were washed with brine and dried over Na_2SO_4 , then the solvent was removed under reduced pressure. The crude product was subjected to column chromatography (0-5% EtAc:Hex). The compound was obtained as a brown oil and its identity confirmed by comparing its 1H NMR spectrum with a reported one.^{S3} 1H NMR (600 MHz, $CDCl_3$) δ 7.93 (d, $J = 2.4$ Hz, 1H), 7.74 (d, $J = 7.7$ Hz, 2H), 7.47 (t, $J = 7.7$ Hz, 2H), 7.35 (t, $J = 7.2$ Hz, 1H), 7.00 (d, $J = 2.5$ Hz, 1H), 4.44 (q, $J = 7.1$ Hz, 2H), 1.42 (t, $J = 7.1$ Hz, 3H) ppm. ESI-MS: m/z found $[M-H]^+$ for $C_{12}H_{13}N_2O_2^+$ 217.13 (calcd. 217.10).

3. NMR Spectroscopy Characterization

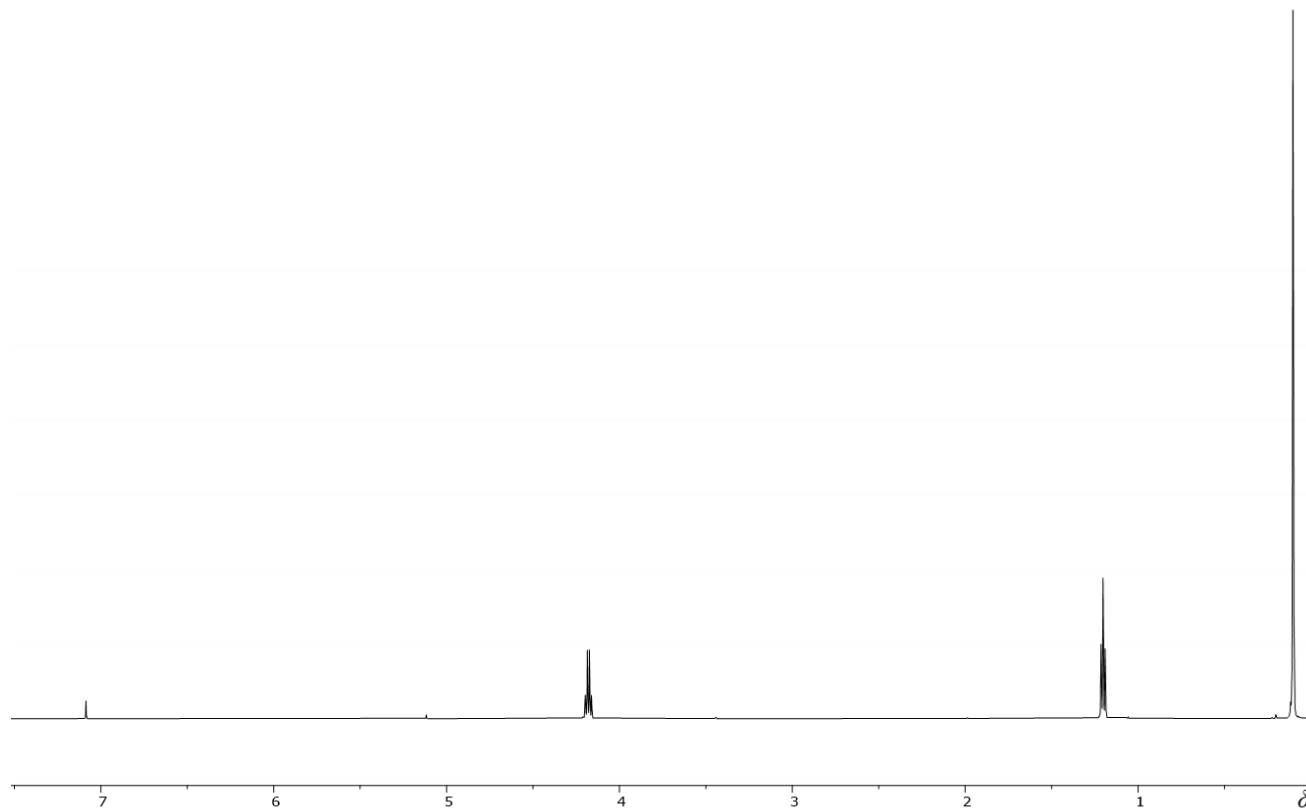


Figure S1. ¹H NMR spectrum of **TMS-alkyne-rotor** in CDCl₃ at 298 K.

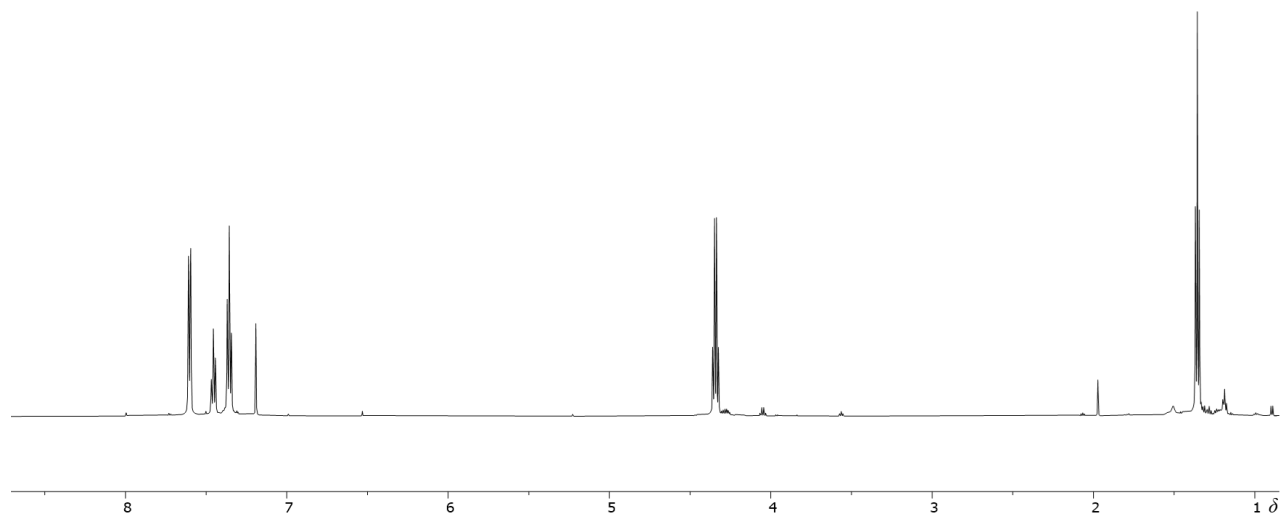


Figure S2. ¹H NMR spectrum of **Ph-alkyne-rotor** in CDCl₃ at 298 K.

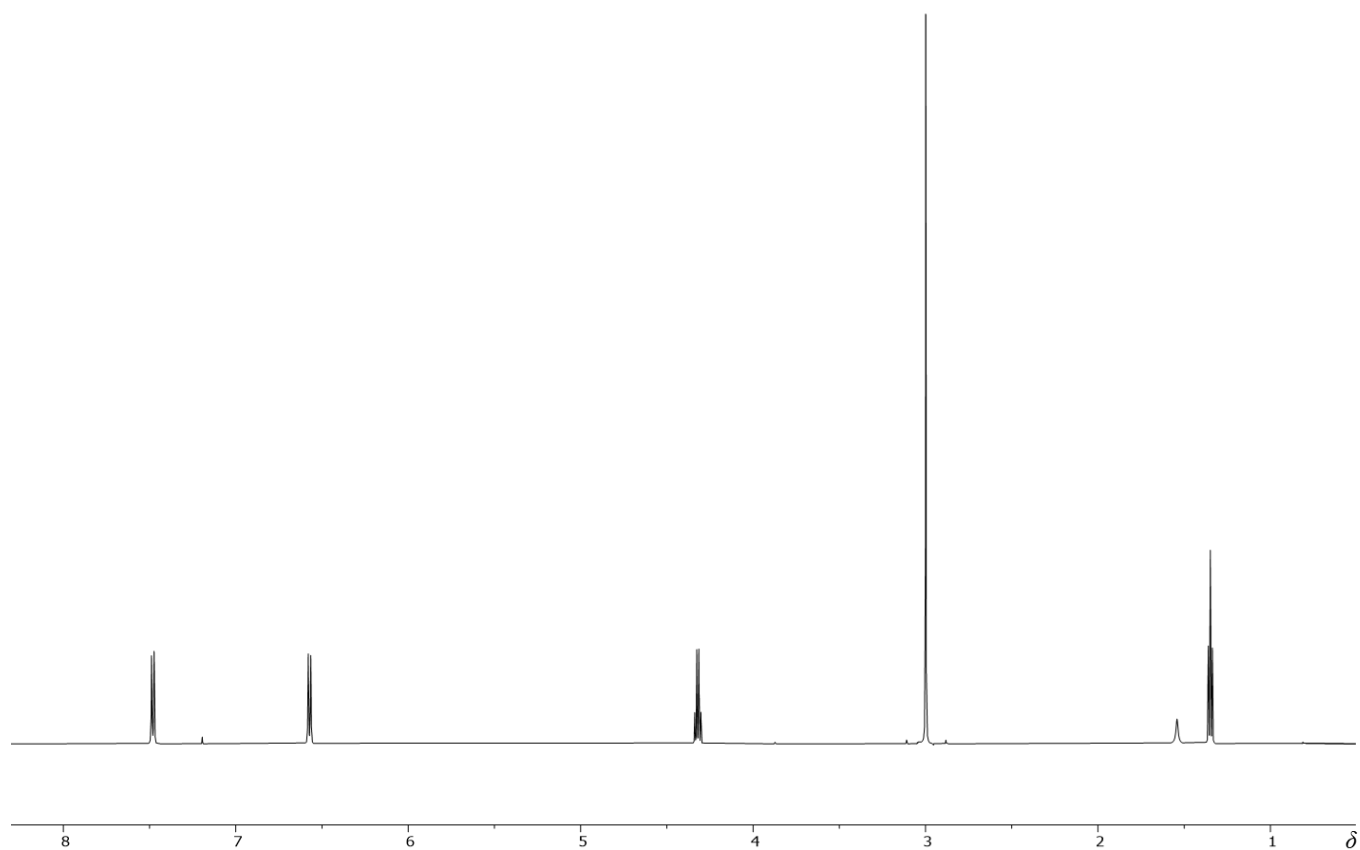


Figure S3. ^1H NMR spectrum of **DMA-alkyne-rotor** in CDCl_3 at 298 K.

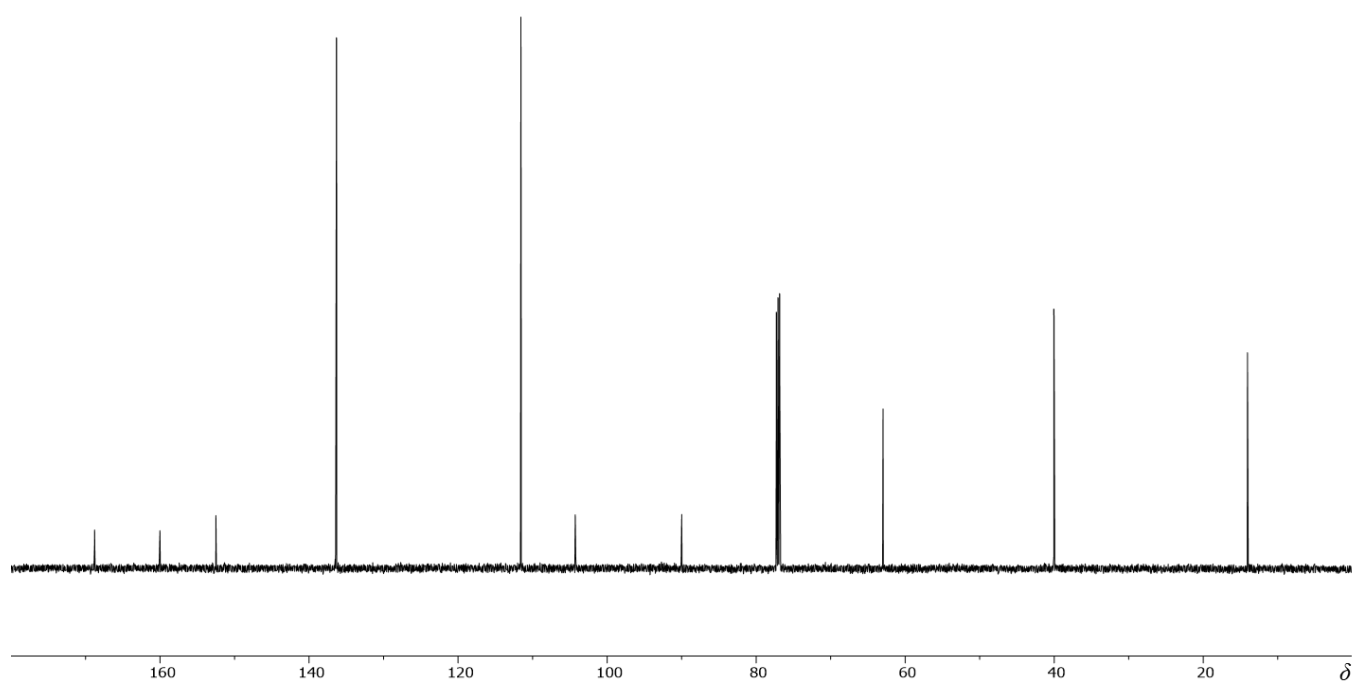


Figure S4. ^{13}C NMR spectrum of **3** in CDCl_3 at 298 K.

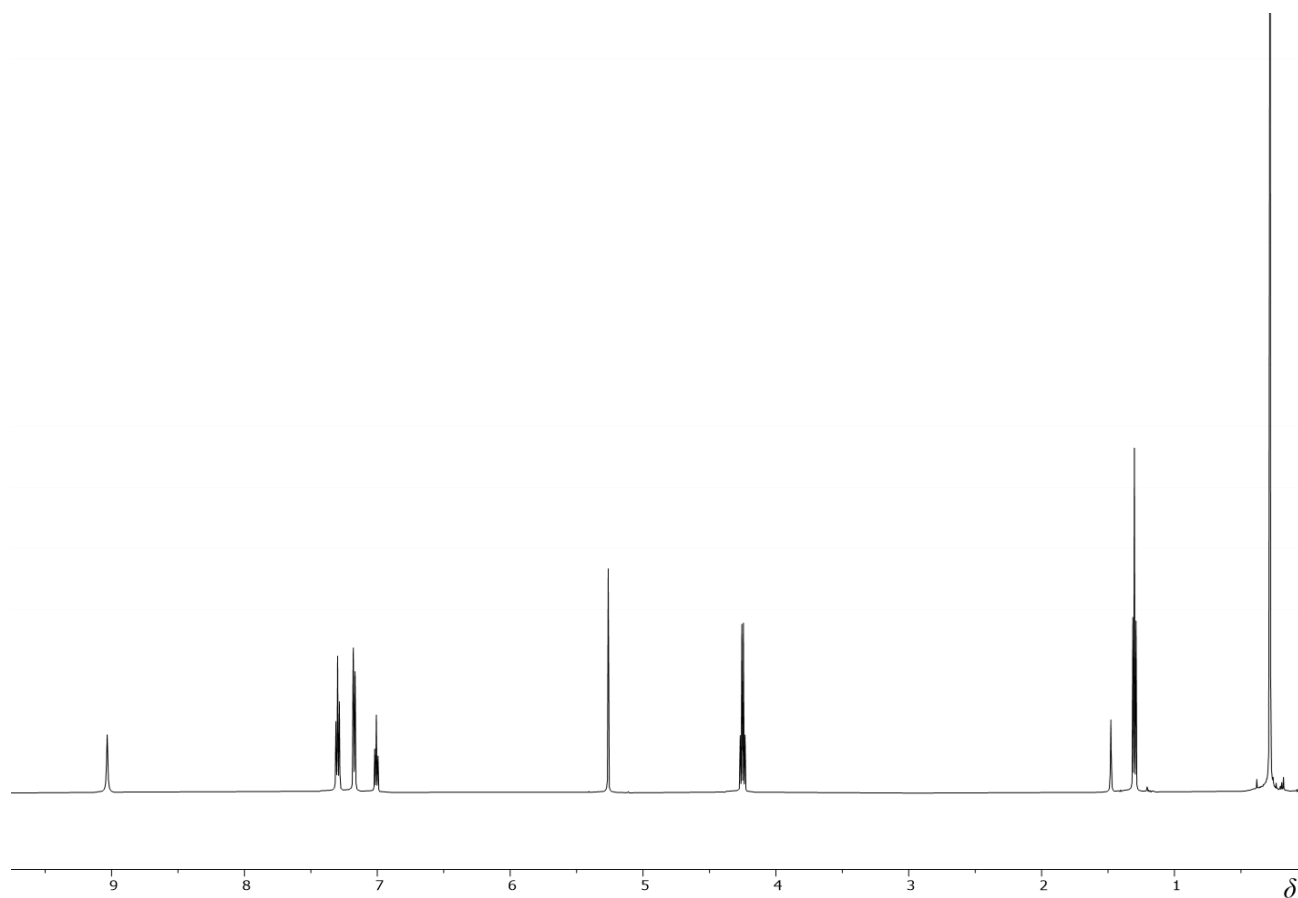


Figure S5. ^1H NMR spectrum of **1** in CD_2Cl_2 at 298 K.

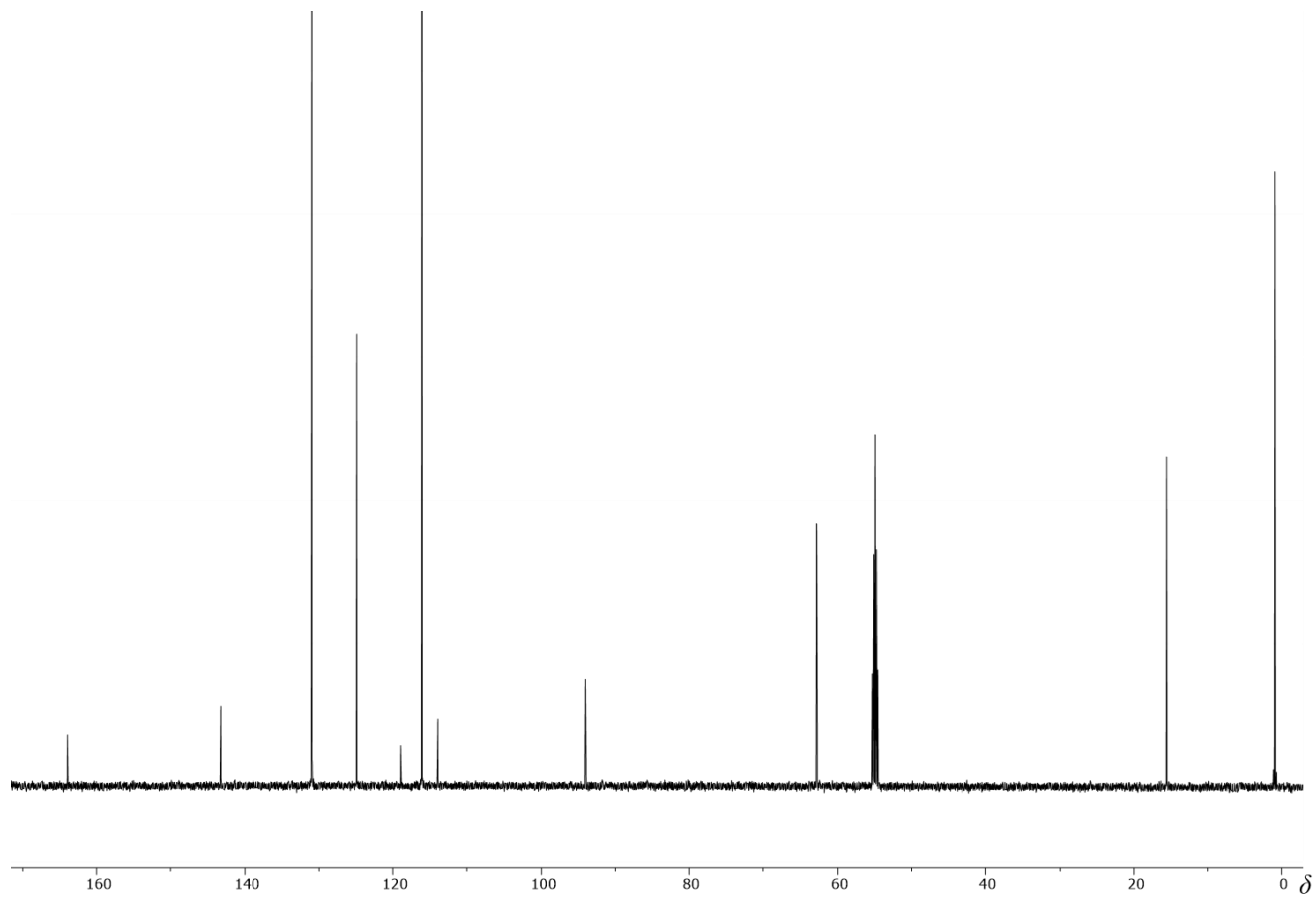


Figure S6. ^{13}C NMR spectrum of **1** in CD_2Cl_2 at 298 K.

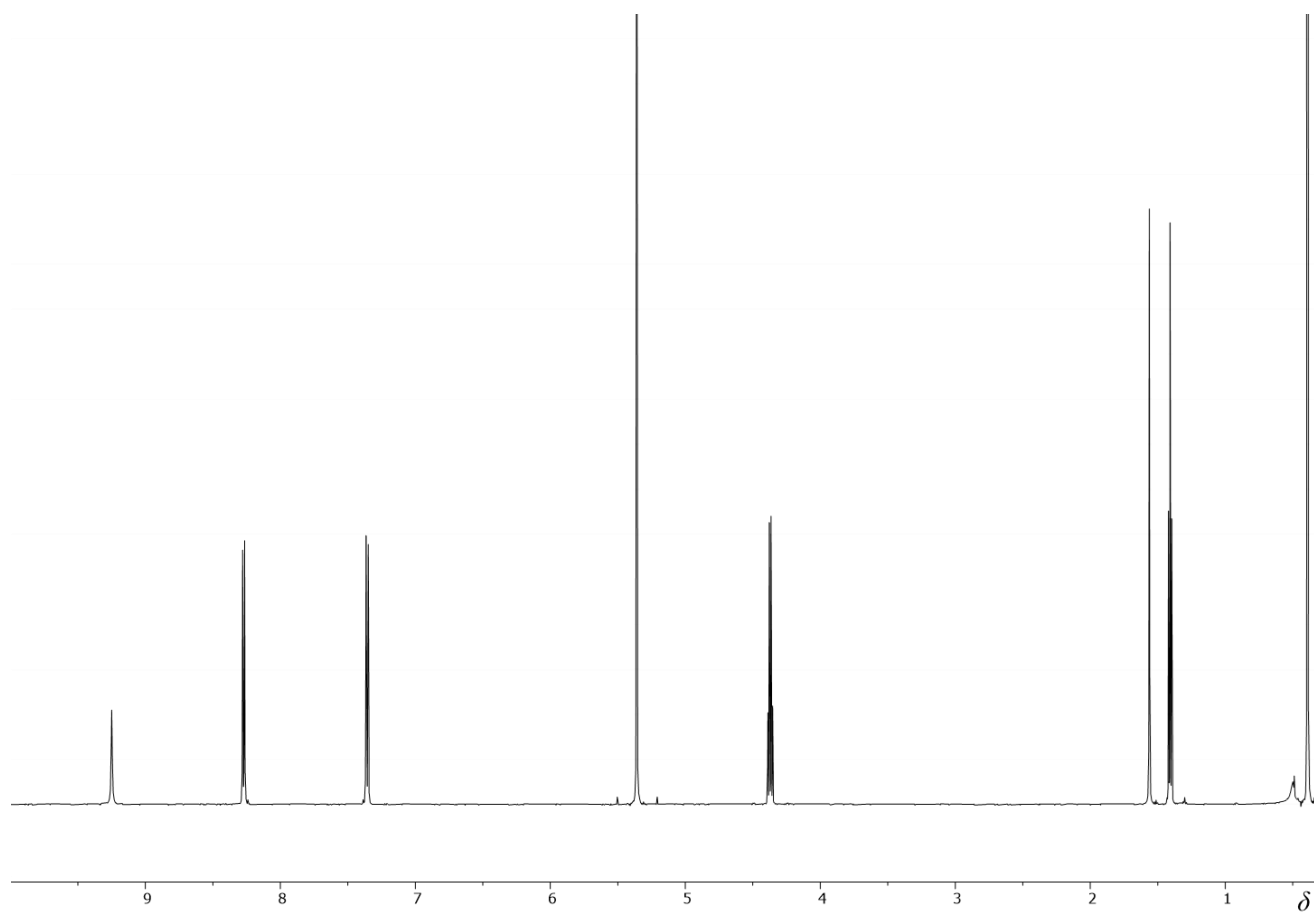


Figure S7. ^1H NMR spectrum of **2** in CD_2Cl_2 at 298 K.

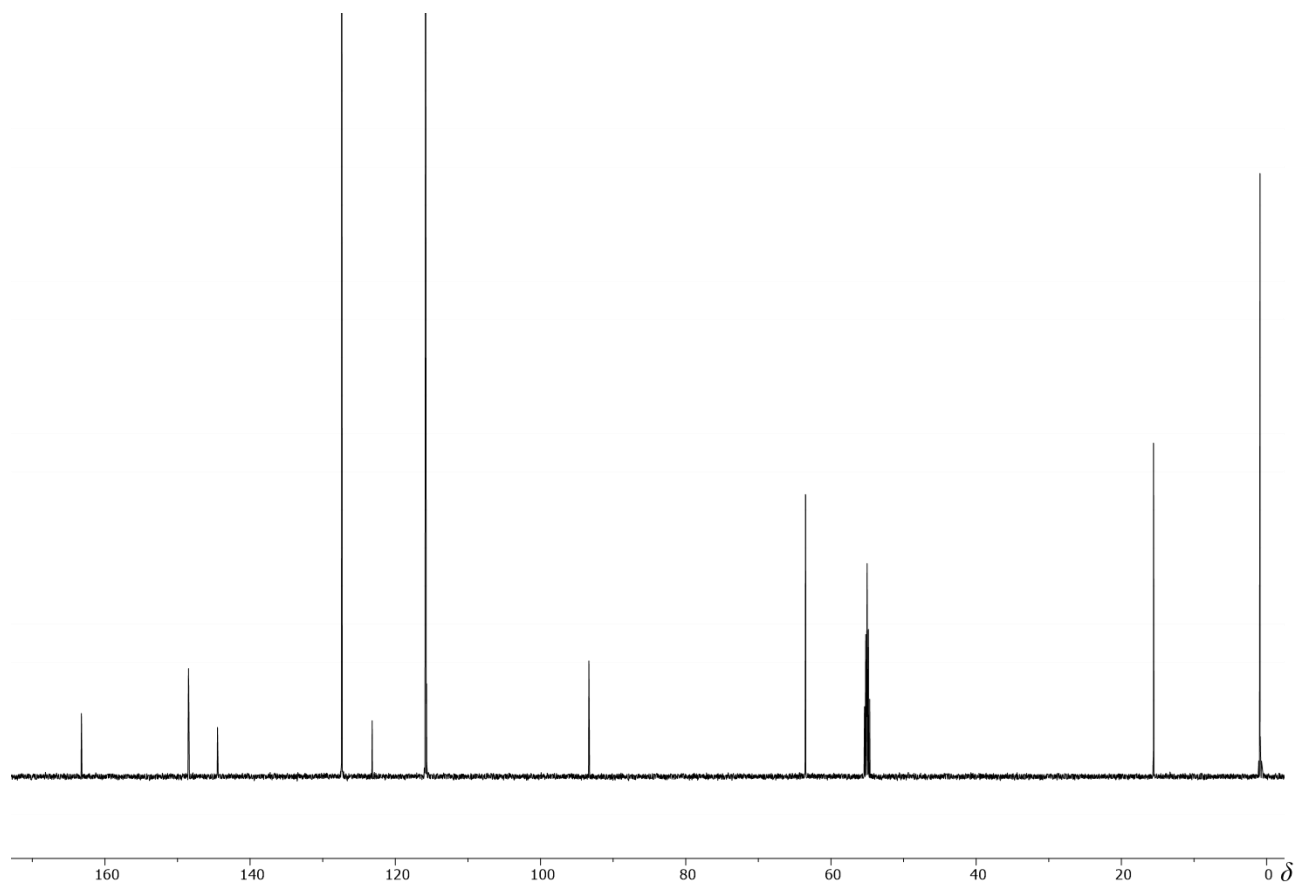


Figure S8. ^{13}C NMR spectrum of **2** in CD_2Cl_2 at 298 K.

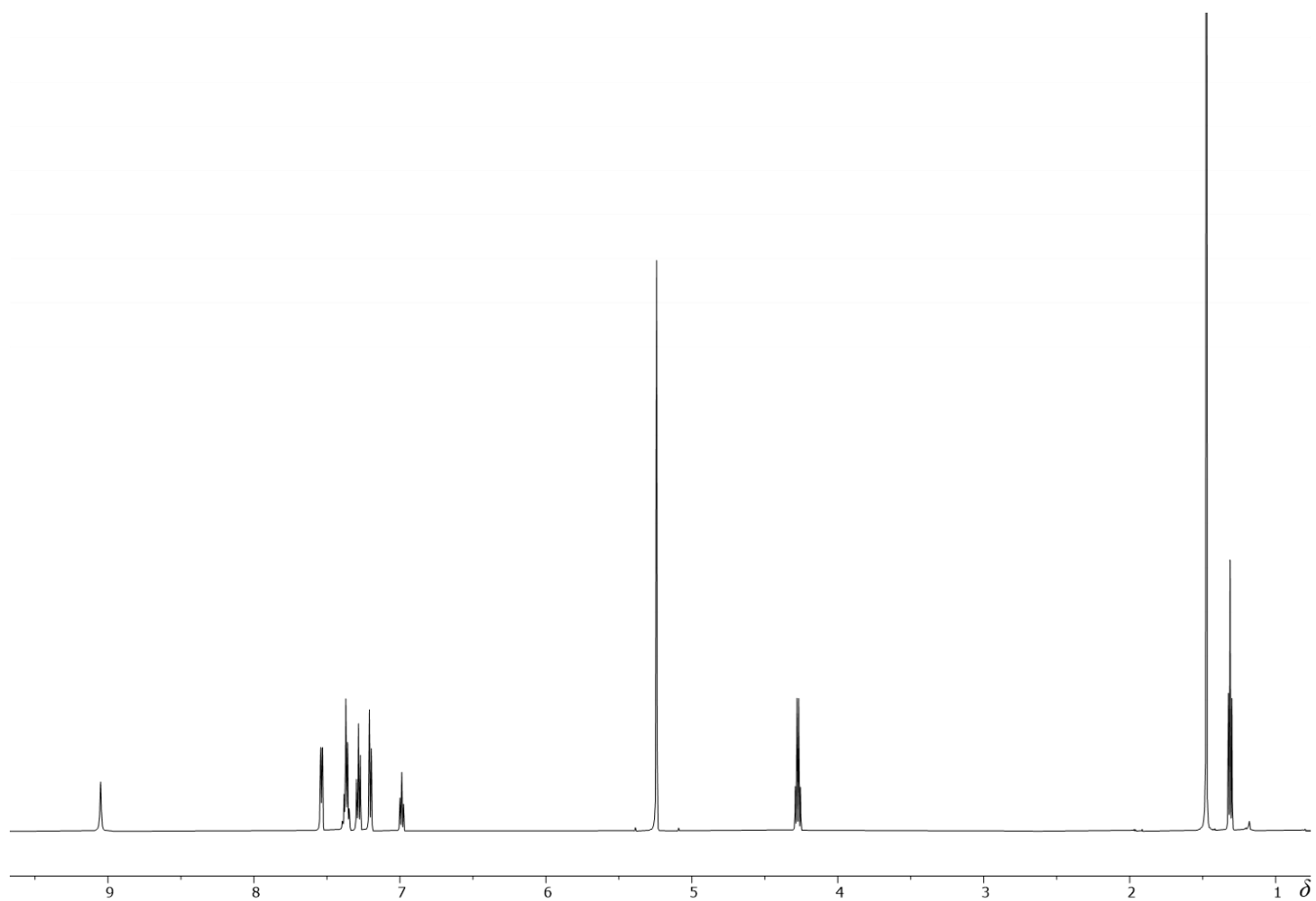


Figure S9. ^1H NMR spectrum of **3** in CD_2Cl_2 at 298 K.

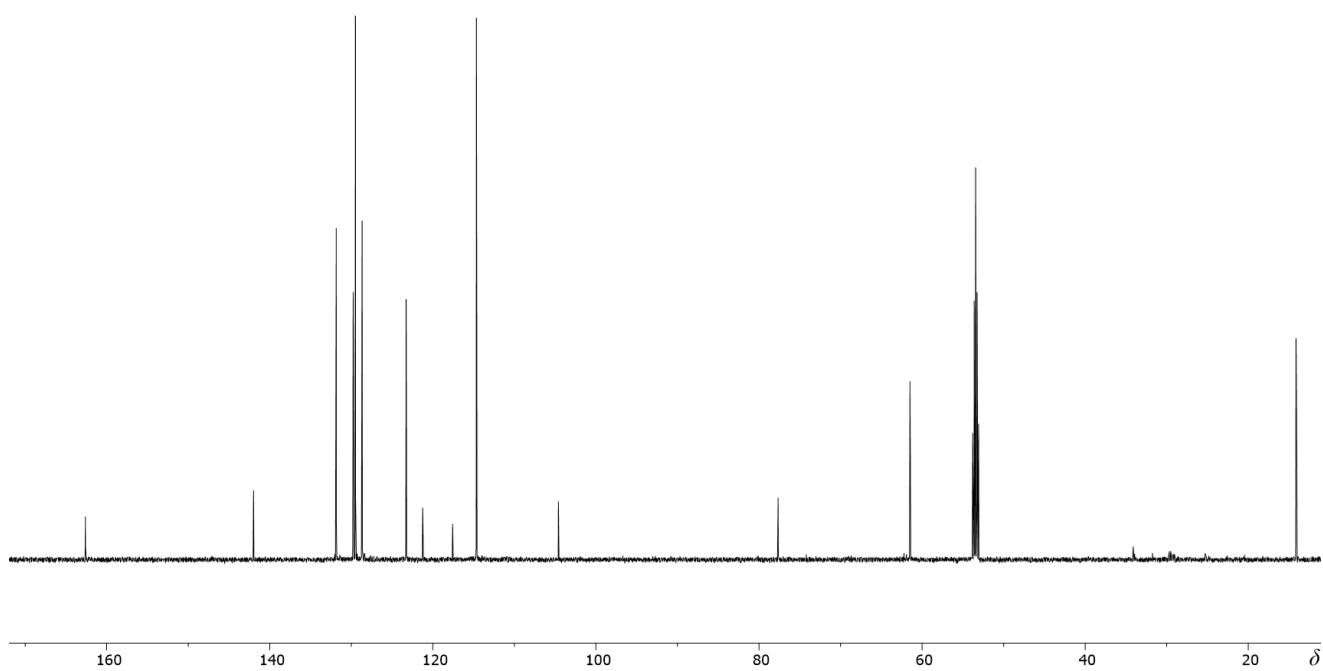


Figure S10. ^{13}C NMR spectrum of **3** in CD_2Cl_2 at 298 K.

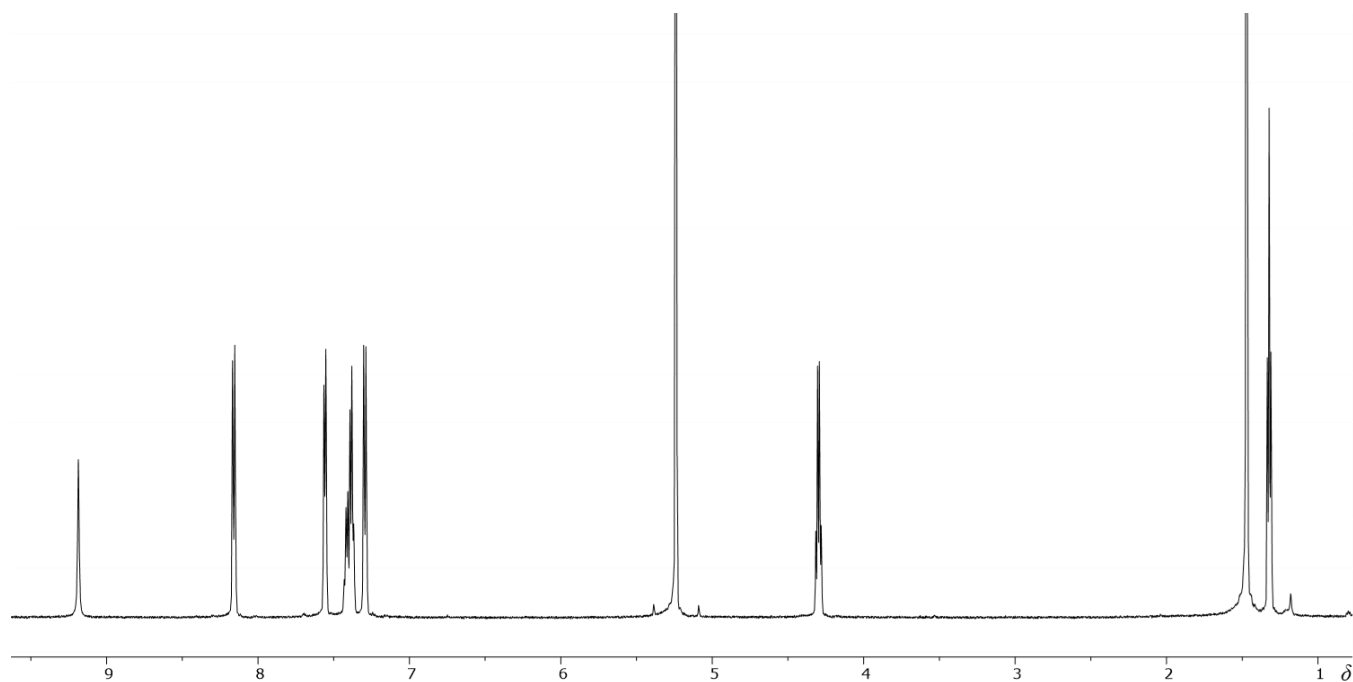


Figure S11. ^1H NMR spectrum of **4** in CD_2Cl_2 at 298 K.

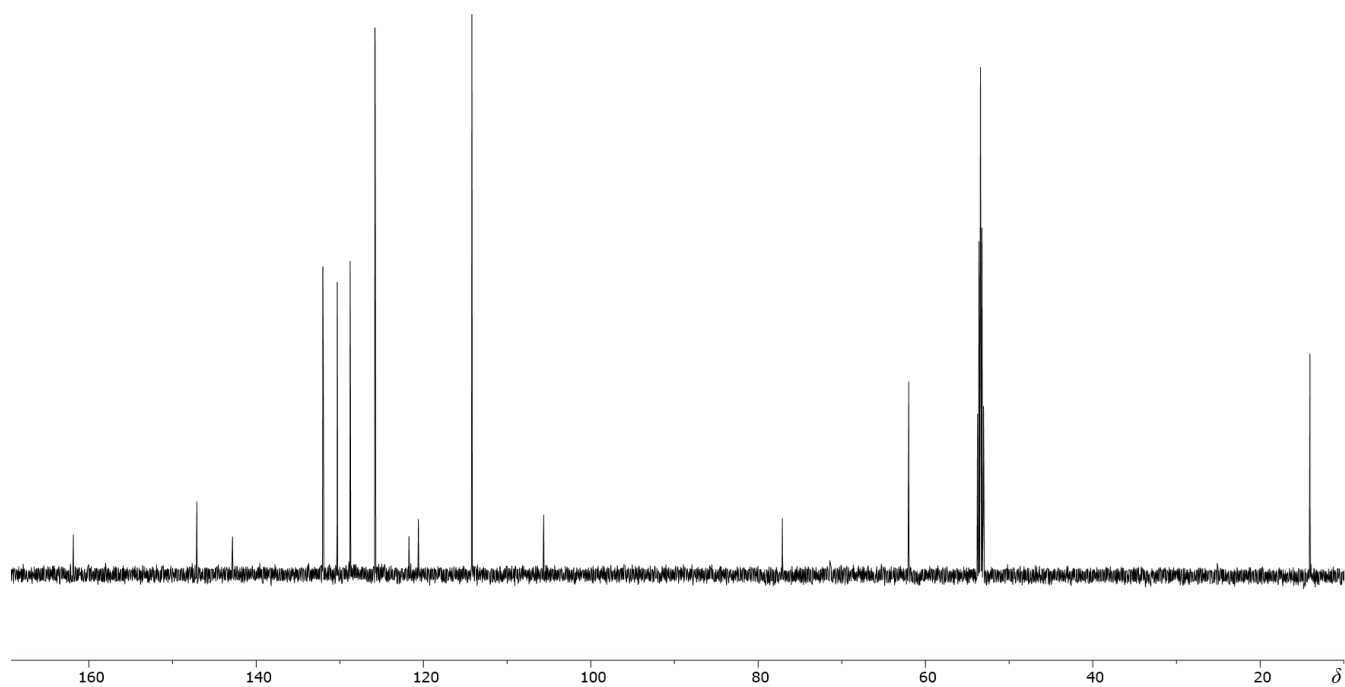


Figure S12. ^{13}C NMR spectrum of **4** in CD_2Cl_2 at 298 K.

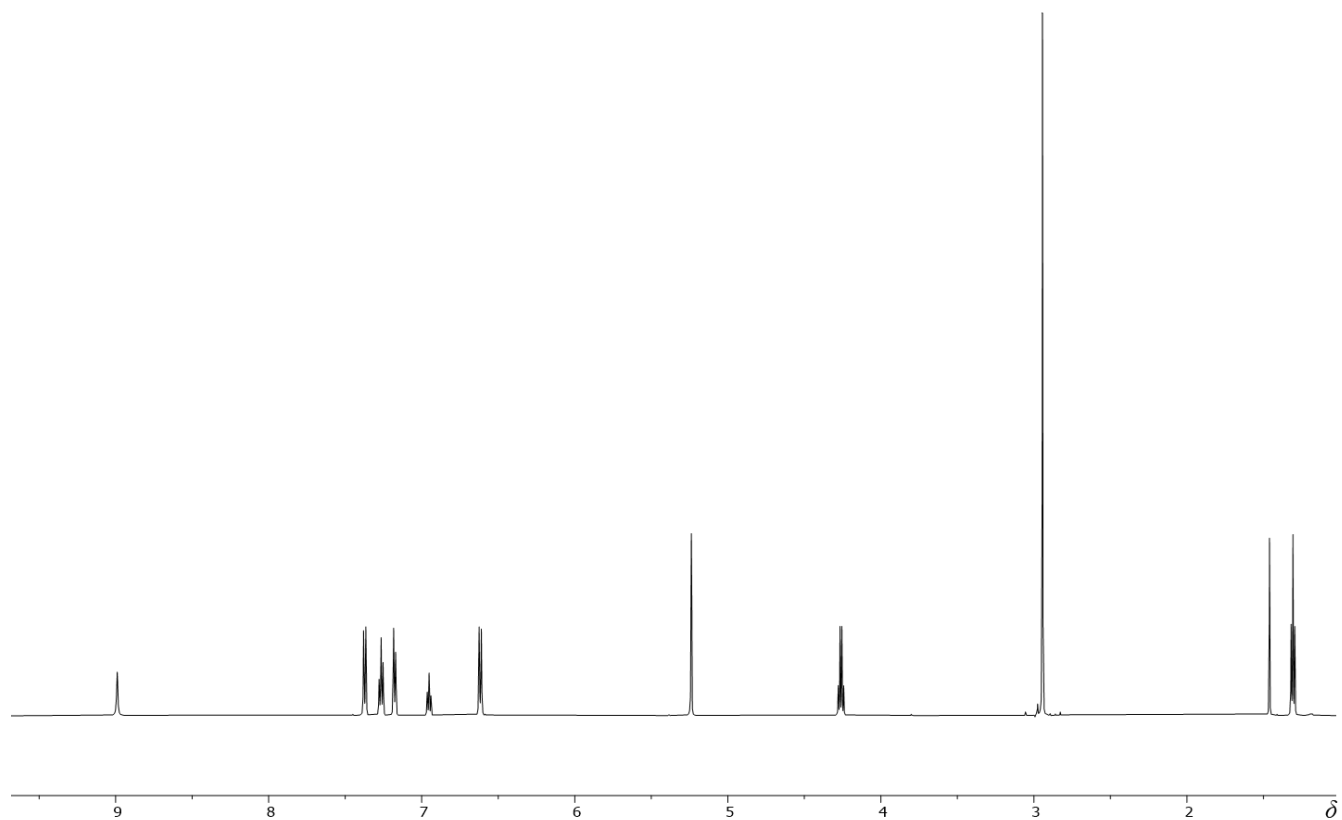


Figure S13. ¹H NMR spectrum of **5** in CD₂Cl₂ at 298 K.

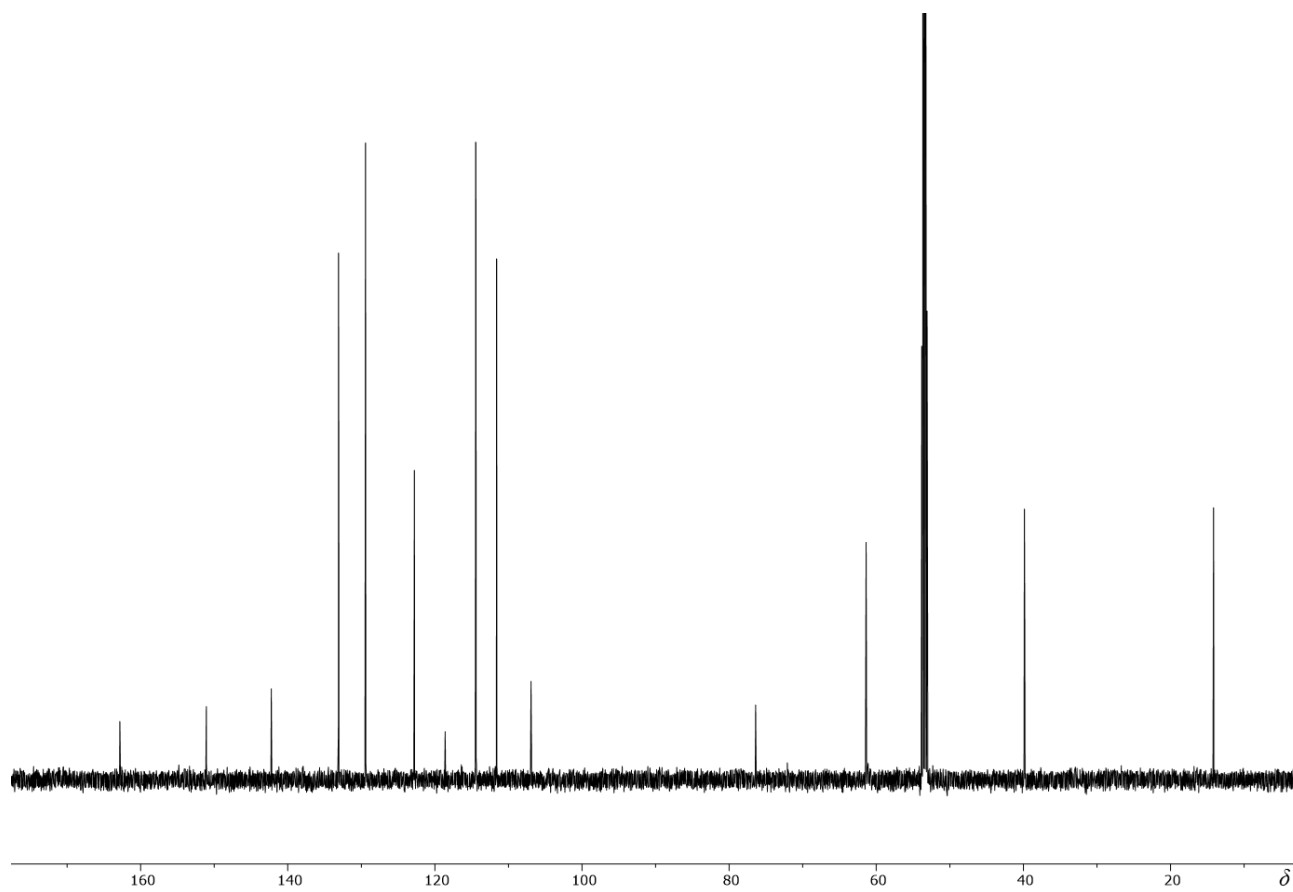


Figure S14. ^{13}C NMR spectrum of **5** in CD_2Cl_2 at 298 K.

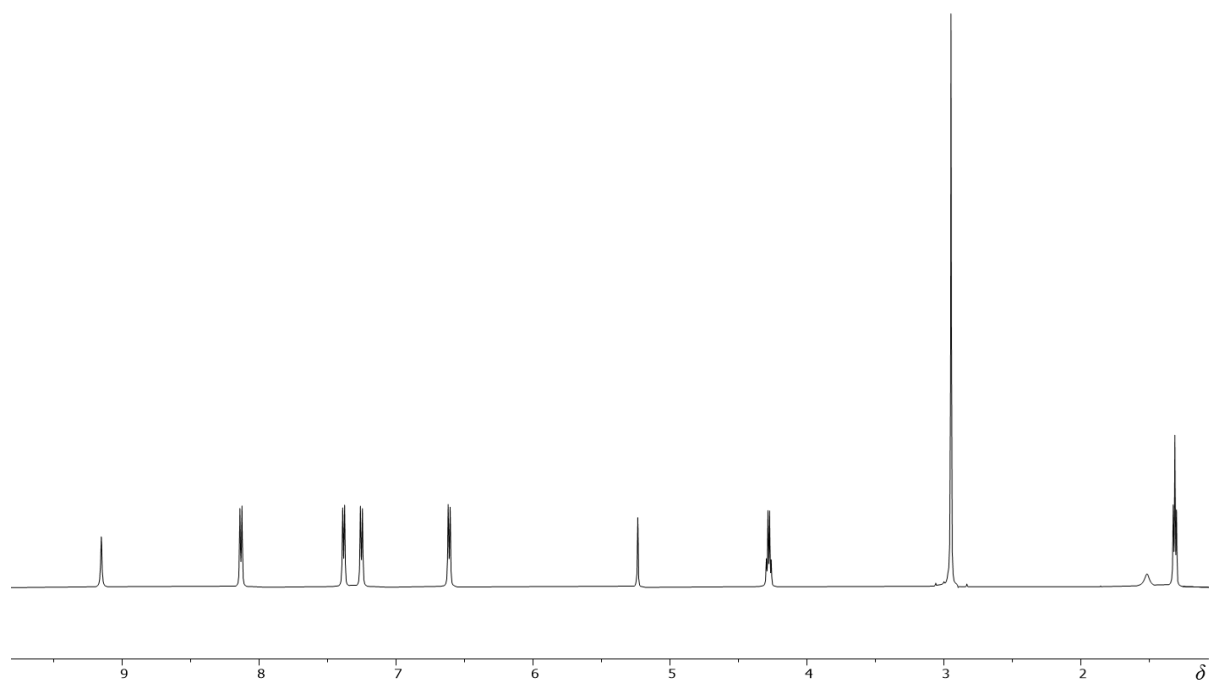


Figure S15. ^1H NMR spectrum of **6** in CD_2Cl_2 at 298 K.

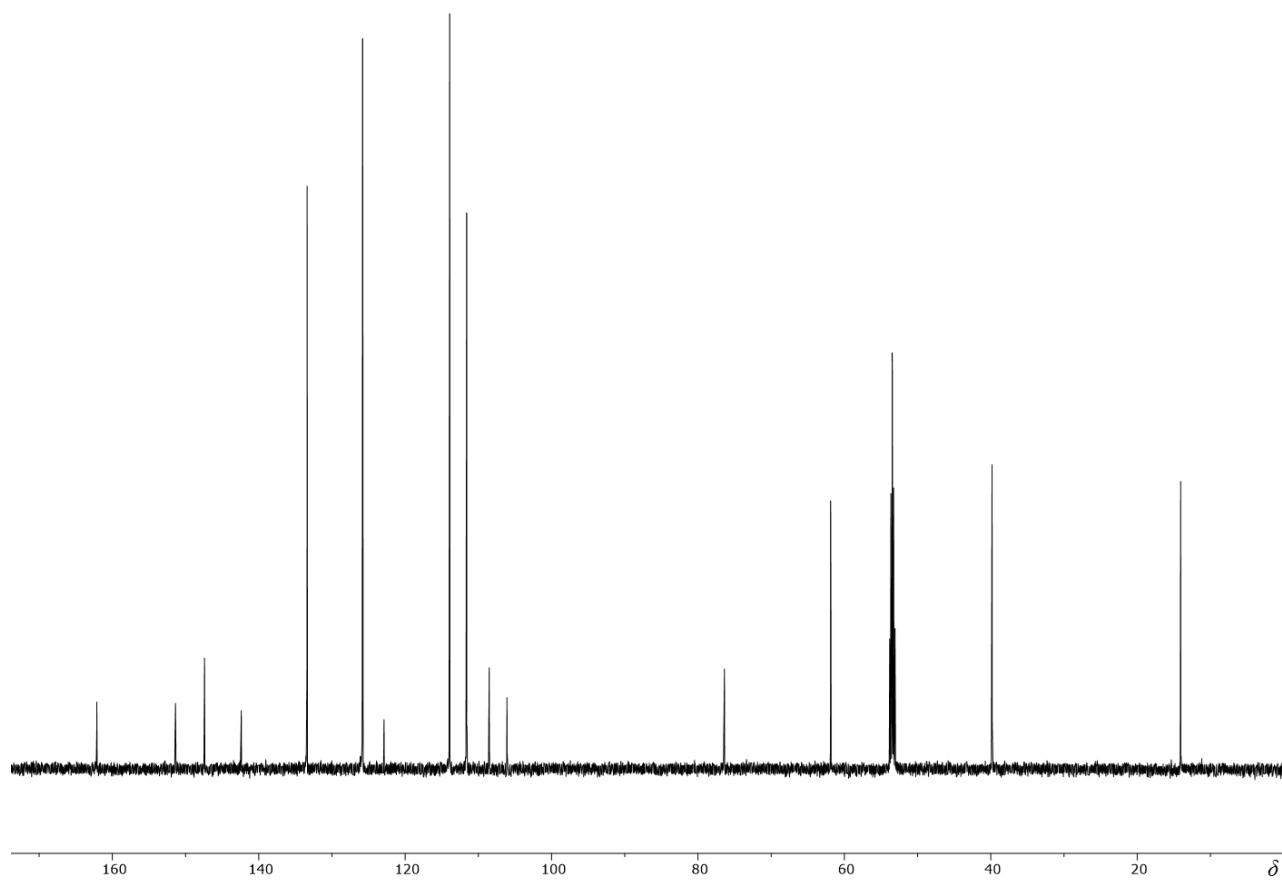


Figure S16. ^{13}C NMR spectrum of **6** in CD_2Cl_2 at 298 K.

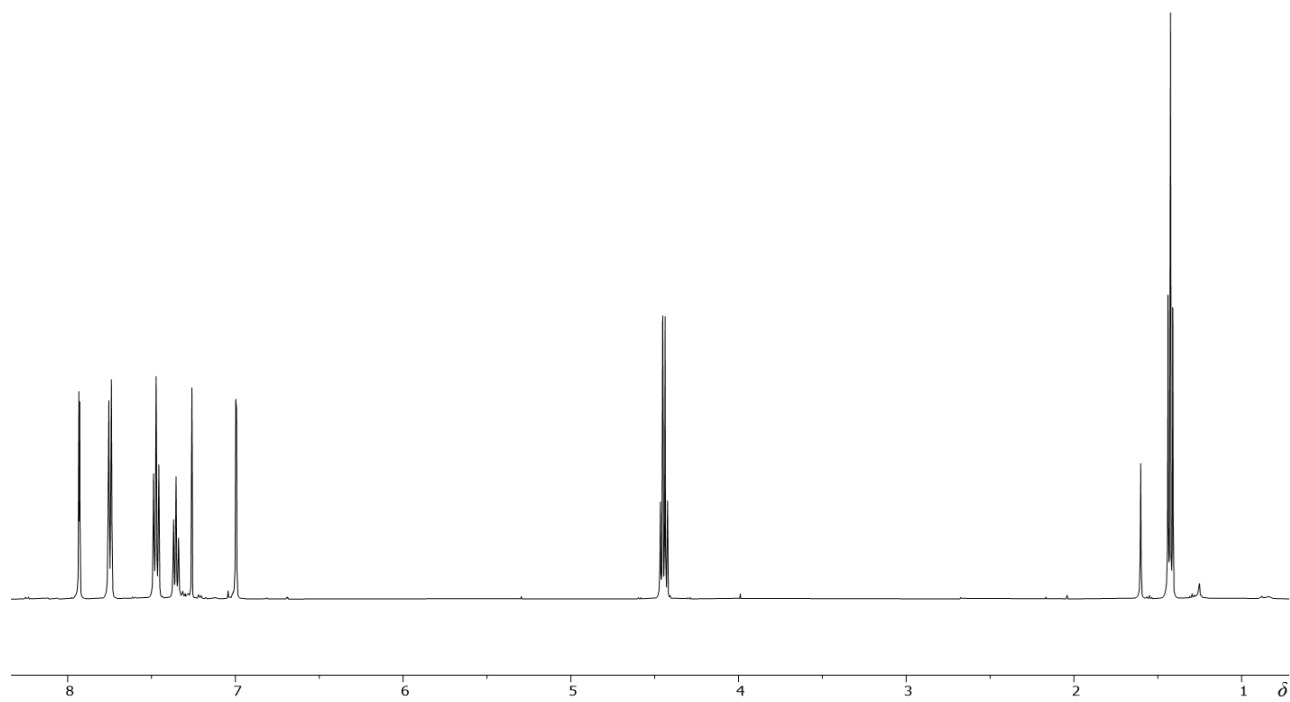


Figure S 17. ^1H NMR spectrum of the pyrazole byproduct in CDCl_3 at 298 K

4. Photoisomerization Studies

The photoisomerization process was studied using UV-Vis and ^1H NMR spectroscopies. For the UV-Vis studies, a 2×10^{-5} M solution (3 mL) of the compound in spectroscopic grade toluene was loaded into a 1 cm quartz cuvette, and the spectra were measured after reaching the appropriate photostationary state (PSS). The isomerization cycles were obtained for hydrazones **1** to **6** by alternating the irradiation at the appropriate wavelengths.

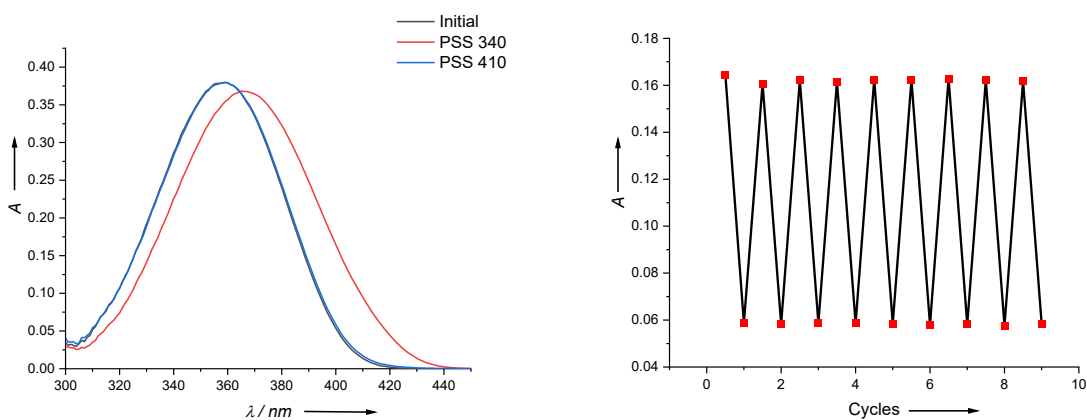


Figure S18. a) Light induced *Z/E* isomerization of **1** (2×10^{-5} M) in toluene. b) Photoisomerization cycles of hydrazone **1** (2×10^{-5} M) in toluene at 294 K. The absorbance change at 387 nm was monitored while alternating the irradiation wavelength between 340 and 410 nm.

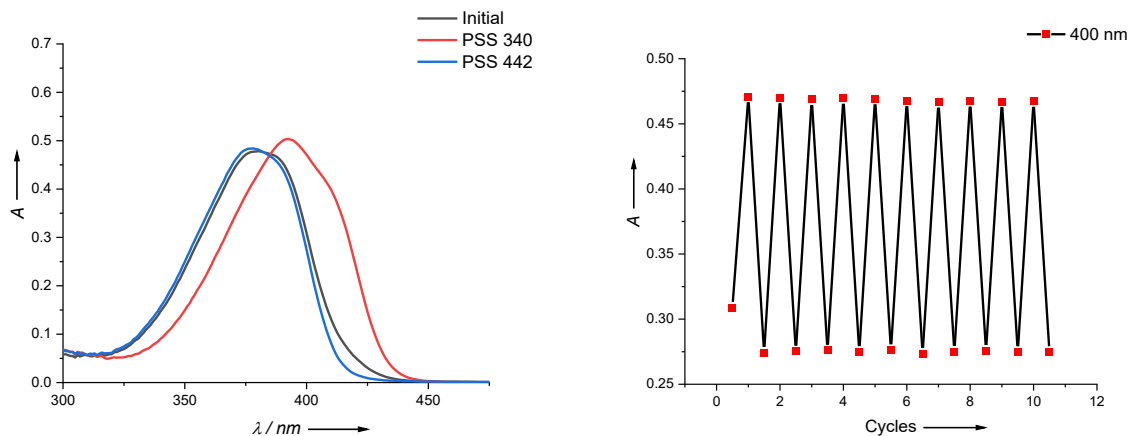


Figure S19. a) Light induced *Z/E* isomerization of **2** (2×10^{-5} M) in toluene. b) Photoisomerization cycles of hydrazone **2** (2×10^{-5} M) in toluene at 294 K. The absorbance change at 400 nm was monitored while alternating the irradiation wavelength between 340 and 442 nm.

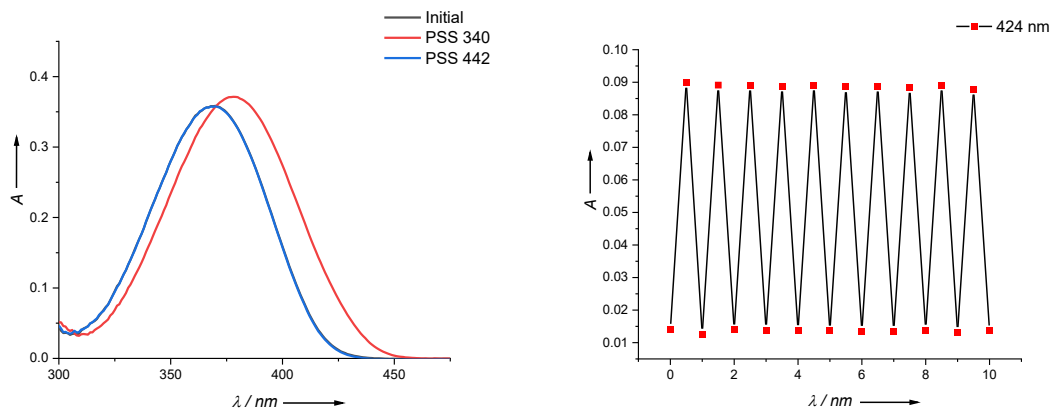


Figure S20. a) Light induced *Z/E* isomerization of **3** (2×10^{-5} M) in toluene. b) Photoisomerization cycles of hydrazone **3** (2×10^{-5} M) in toluene at 294 K. The absorbance change at 424 nm was monitored while alternating the irradiation wavelength between 340 and 442 nm.

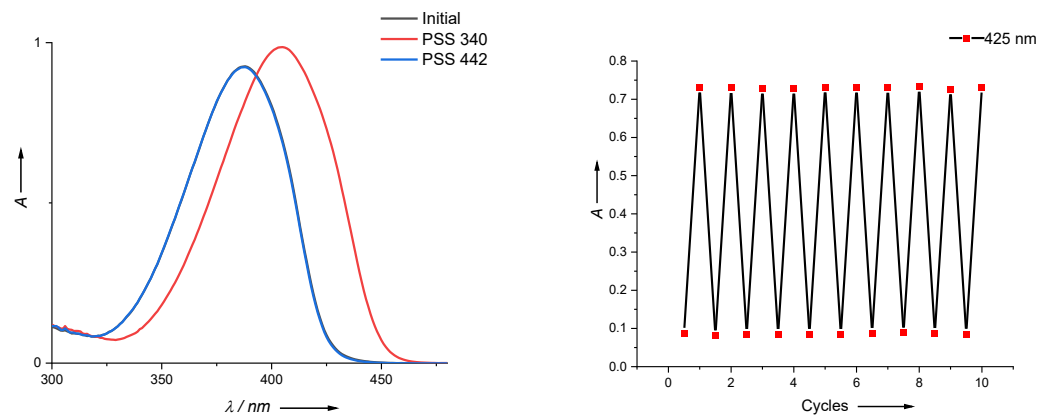


Figure S21. a) Light induced *Z/E* isomerization of **4** (2×10^{-5} M) in toluene. b) Photoisomerization cycles of hydrazone **4** (2×10^{-5} M) in toluene at 294 K. The absorbance change at 425 nm was monitored while alternating the irradiation wavelength between 340 and 442 nm.

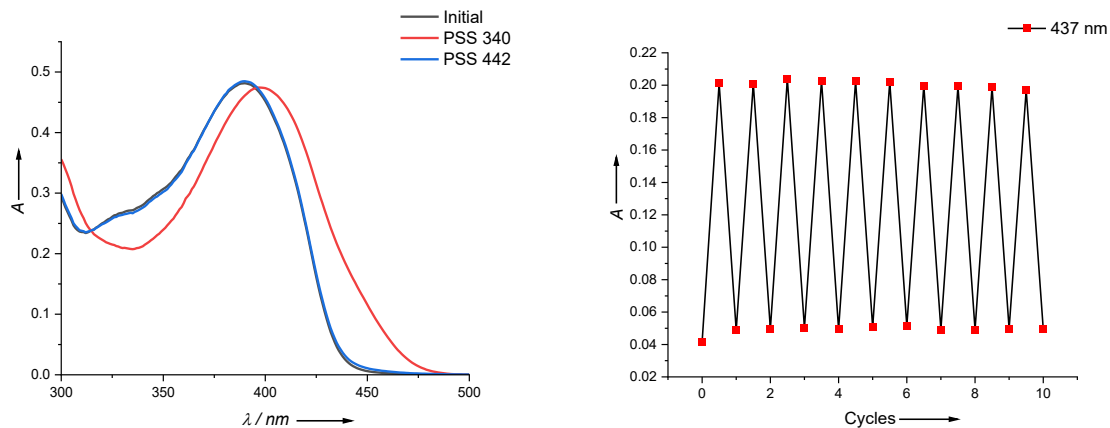


Figure S22. a) Light induced *Z/E* isomerization of **5** (2×10^{-5} M) in toluene. b) Photoisomerization cycles of hydrazone **5** (2×10^{-5} M) in toluene at 294 K. The absorbance change at 437 nm was monitored while alternating the irradiation wavelength between 340 and 442 nm.

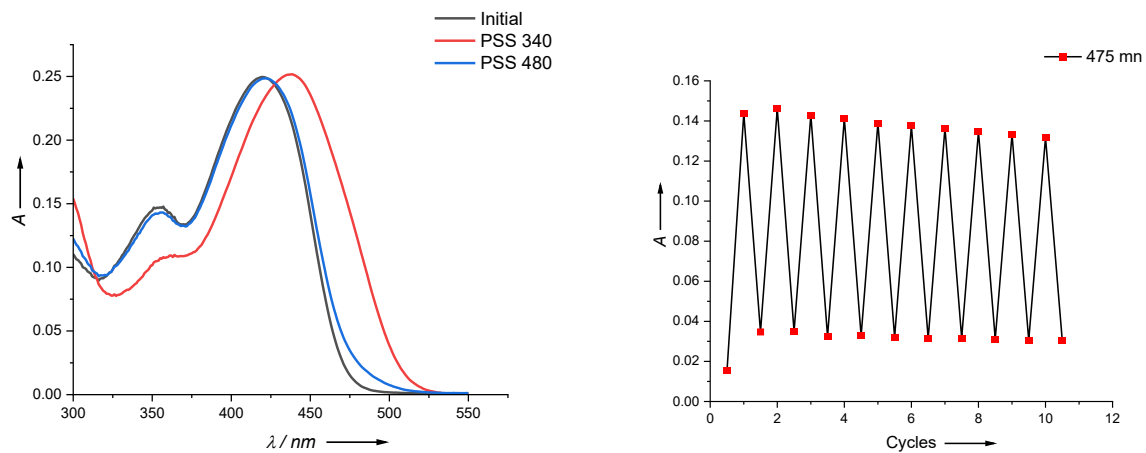


Figure S23. a) Light induced *Z/E* isomerization of **6** (2×10^{-5} M) in toluene. b) Photoisomerization cycles of hydrazone **6** (2×10^{-5} M) in toluene at 294 K. The absorbance change at 475 nm was monitored while alternating the irradiation wavelength between 340 and 480 nm.

5. Photostationary States Studies

The PSSs were determined using ^1H NMR spectroscopy. Solutions (1×10^{-3} M) of hydrazones **1** to **6** in toluene- d_8 were irradiated with the appropriate wavelength until no changes in the ^1H NMR spectra were observed with continued irradiation. The *E* and *Z* isomer ratios were determined by integrating the CH_2 quartet signals.

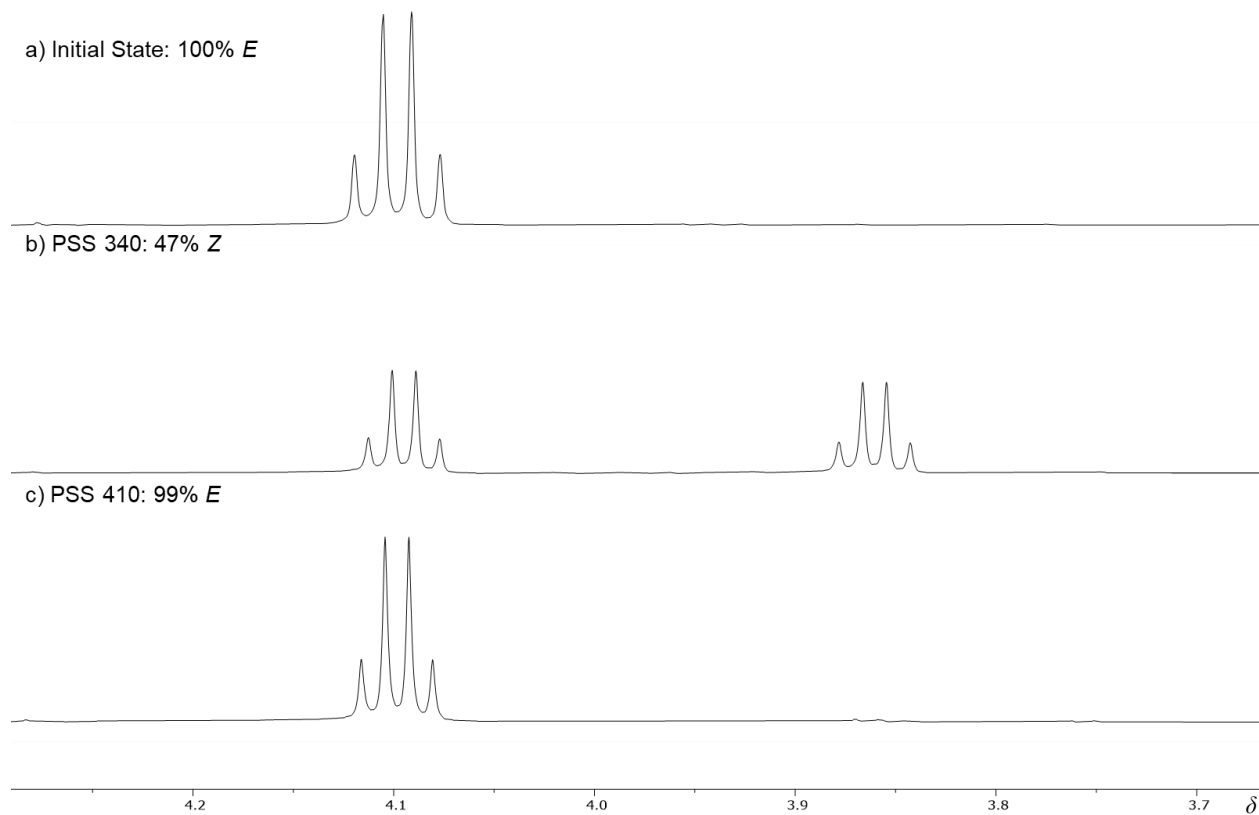


Figure S24. ^1H NMR spectra (toluene- d_8 , 298 K) of **1** a) before, and b) after 340 nm, c) followed by 410 nm photoirradiation to reach the appropriate PSSs.

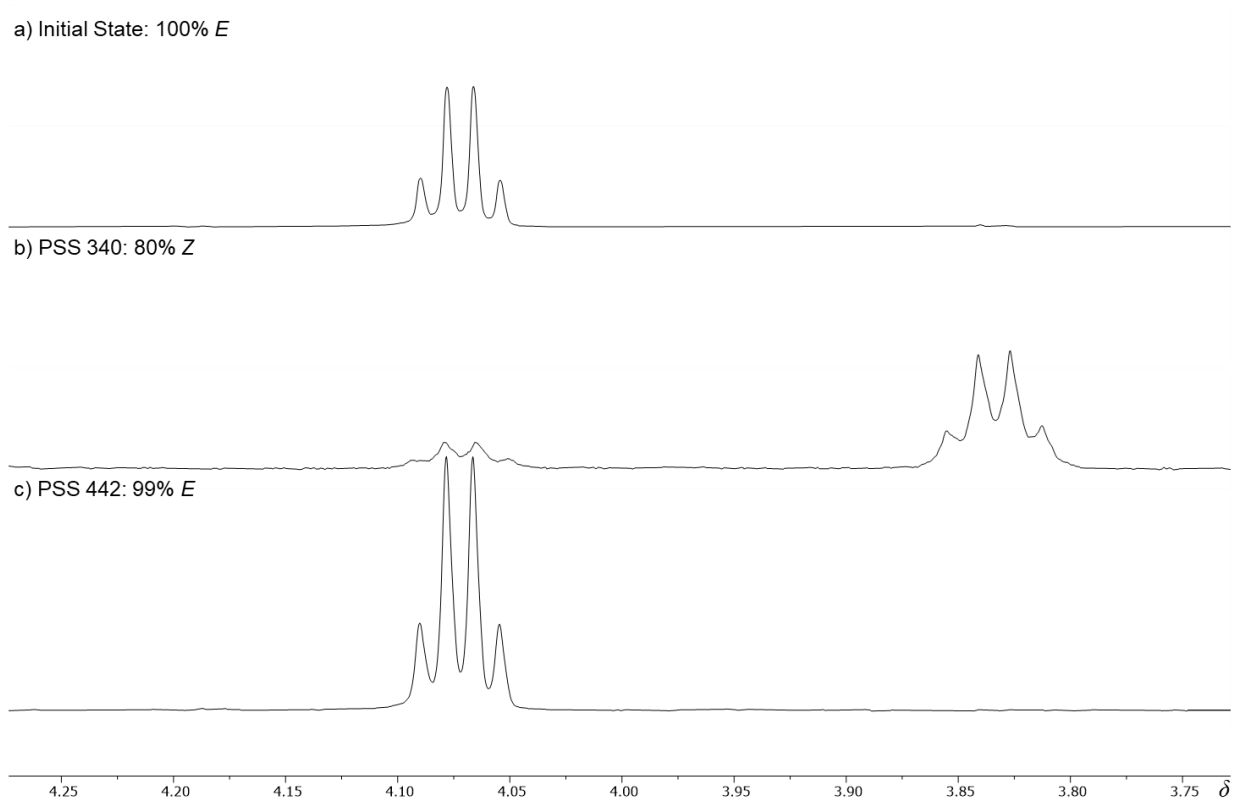


Figure S25. ^1H NMR spectra (toluene- d_8 , 298 K) of **2** a) before, and b) after 340 nm, c) followed by 442 nm photoirradiation to reach the appropriate PSSs.

a) Initial State: 96% *E*



b) PSS 340: 43% *Z*



c) PSS 410: 94% *E*

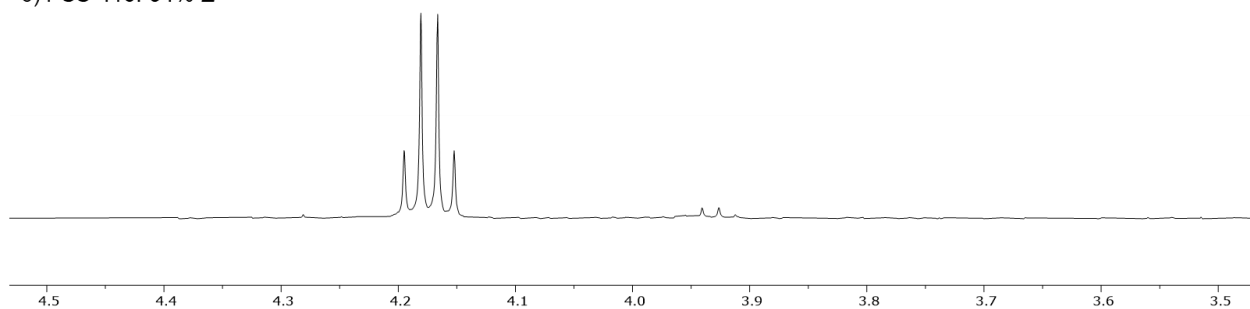


Figure S26. ^1H NMR spectra (toluene- d_8 , 298 K) of **3** a) before, and b) after 340 nm, c) followed by 410 nm photoirradiation to reach the appropriate PSSs.

a) Initial State: >99% *E*

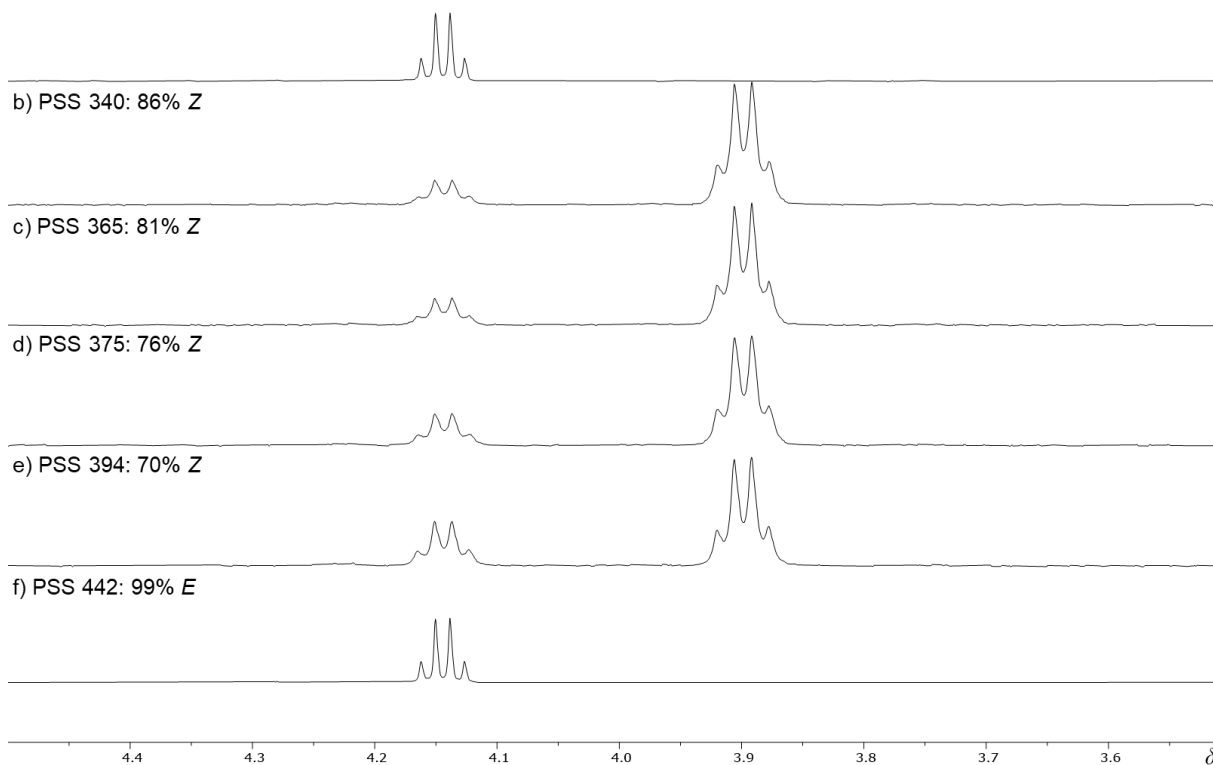


Figure S27. ¹H NMR spectra (toluene-*d*₈, 298 K) of **4** a) before, and b) after 340 nm followed by c) 365 nm; d) 375 nm; e) 394 nm and f) 442 nm photo irradiation to reach the appropriate PSSs.

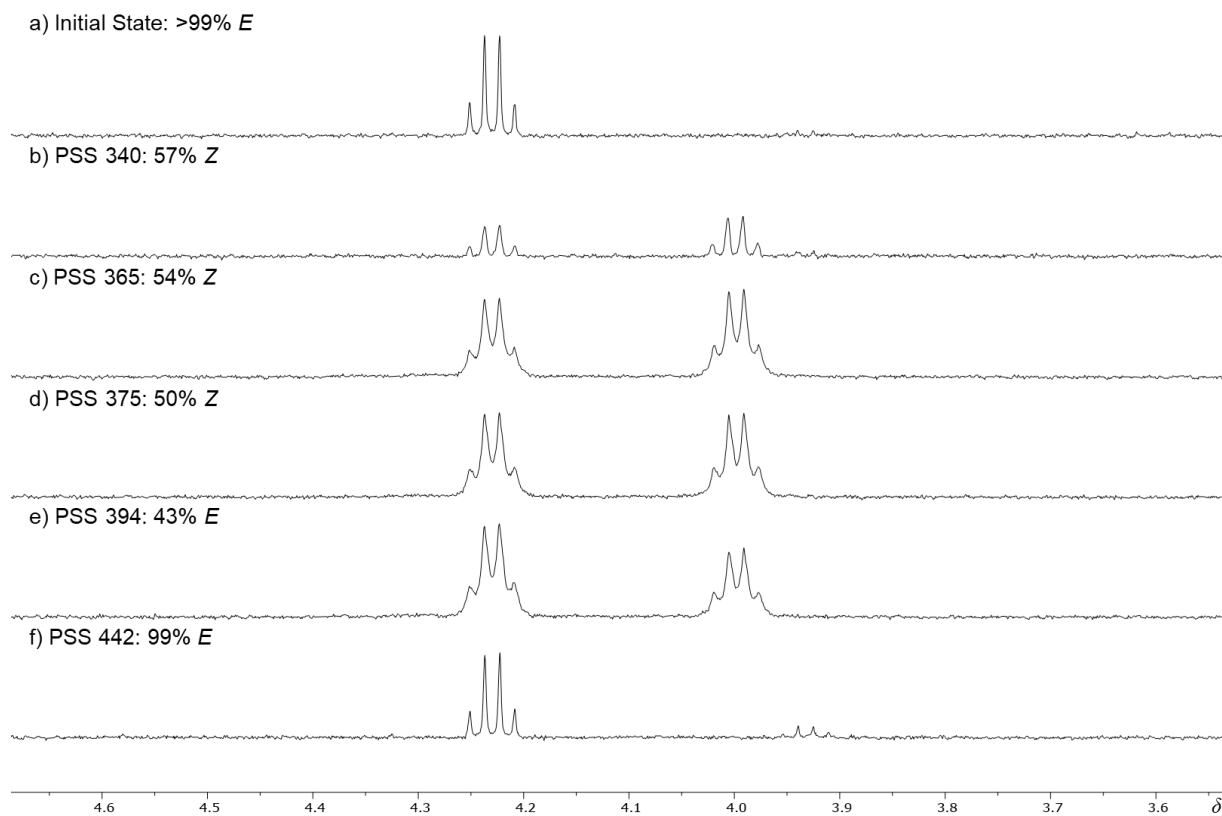


Figure S28. ¹H NMR spectra (toluene-*d*₈, 298 K) of **5** a) before, and b) after 340 nm followed by c) 365 nm; d) 375 nm; e) 394 nm and f) 442 nm photo irradiation to reach the appropriate PSSs (small peaks appear due to photodegradation)

a) Initial State: >99% *E*



b) PSS 340: 75% *Z*



c) PSS 480: 87% *E*



Figure S29. ^1H NMR spectra (toluene- d_8 , 298 K) of **6** a) before, and b) after 340 nm followed by c) 480 nm photo irradiation to reach the appropriate PSS.

6. Photoisomerization Quantum Yield of Alkyne Hydrazones.

The quantum yield (Φ) of all the derivatives was determined by following a previously reported procedure.^{S4} To describe the kinetic behavior of the isomerization process, we used a first-order kinetic model. The rate of conversion of the *E* isomer to the *Z* isomer is governed by equation 1. Actinometry was performed to determine the flux of light from the irradiation system. A 1×10^{-5} M solution of each of the derivatives in spectroscopic grade toluene was irradiated with 340 nm light. The absorbance intensity at a specific wavelength was measured as a function of time. These values were then used to calculate the integrated photokinetic factor $x(t)$ (equation 2). The resulting values of $x(t)$ were plotted against the fraction of the *Z* isomer (y), which was determined using UV-Vis spectroscopy, and the PSS isomer ratio obtained from ^1H NMR spectroscopy (Figures S27–S31). This plot was fitted using Equation 4 to determine R (equation 3) which is the kinetic rate factor.

$$\ln \frac{y_{\infty} - y}{y_{\infty} - y_0} = - \frac{I \cdot l \cdot \Phi_{E \rightarrow Z} \cdot \epsilon_E}{V \cdot y_{\infty}} \int_{t_0}^t \frac{1 - 10^{-A(t)}}{A(t)} dt \quad \text{Eq. 1}$$

$$x(t) = \int_{t_0}^t \frac{1 - 10^{-A(t)}}{A(t)} dt \quad \text{Eq. 2}$$

$$R = - \frac{I \cdot l \cdot \Phi_{E \rightarrow Z} \cdot \epsilon_E}{V \cdot y_{\infty}} \quad \text{Eq. 3}$$

where $A(t)$ is defined as absorption at time t , V indicates the volume of solution, y_{∞} is the *Z* isomer fraction at the PSS and y_0 is the *Z* isomer fraction at $t=0$ s, I_0 indicates the molar flux of light, ϵ_E indicates the molar absorptivity and l indicates the path length.

The resulting function was fitted using

$$y = y_{\infty} + Ae^{Rt} \quad \text{Eq. 4}$$

From this, the quantum yield $\Phi_{E \rightarrow Z}$ was determined using:

$$\Phi_{E \rightarrow Z} = \frac{R \cdot V \cdot y_{\infty}}{I_0 \cdot \epsilon_E \cdot l} \quad \text{Eq. 5}$$

Typical fits are shown in Figures S24-S28. The resulting value for R was used in equation 5 to determine $\Phi_{E \rightarrow Z}$. The process was repeated using 410 nm light to measure $\Phi_{Z \rightarrow E}$.

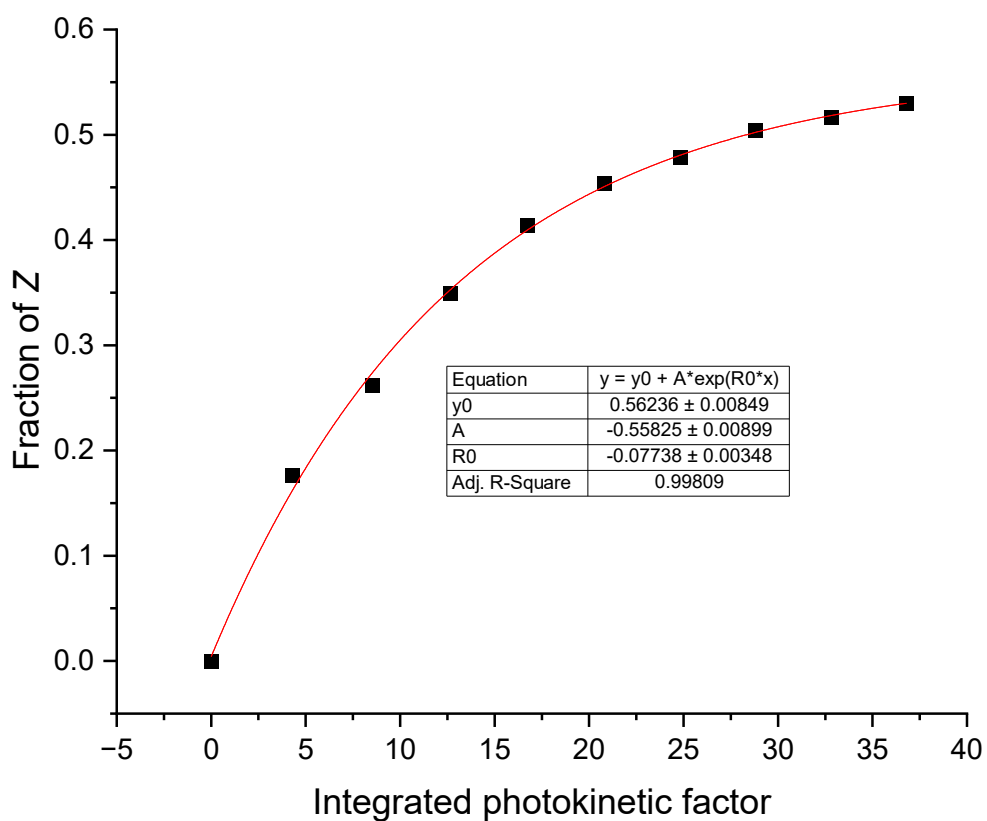


Figure S30. Exponential fitting of the Z isomer fraction against integrated photokinetic factor $x(t)$. $\epsilon_{1-E@340 \text{ nm}} = 2,200 \text{ M}^{-1} \cdot \text{cm}^{-1}$ was used for quantum yield calculations. The photoisomerization quantum yield of **1-E** to **1-Z** in toluene ($1 \times 10^{-5} \text{ M}$) at 298 K was calculated to be $8.4 \pm 1.1 \%$ based on three consecutive measurements.

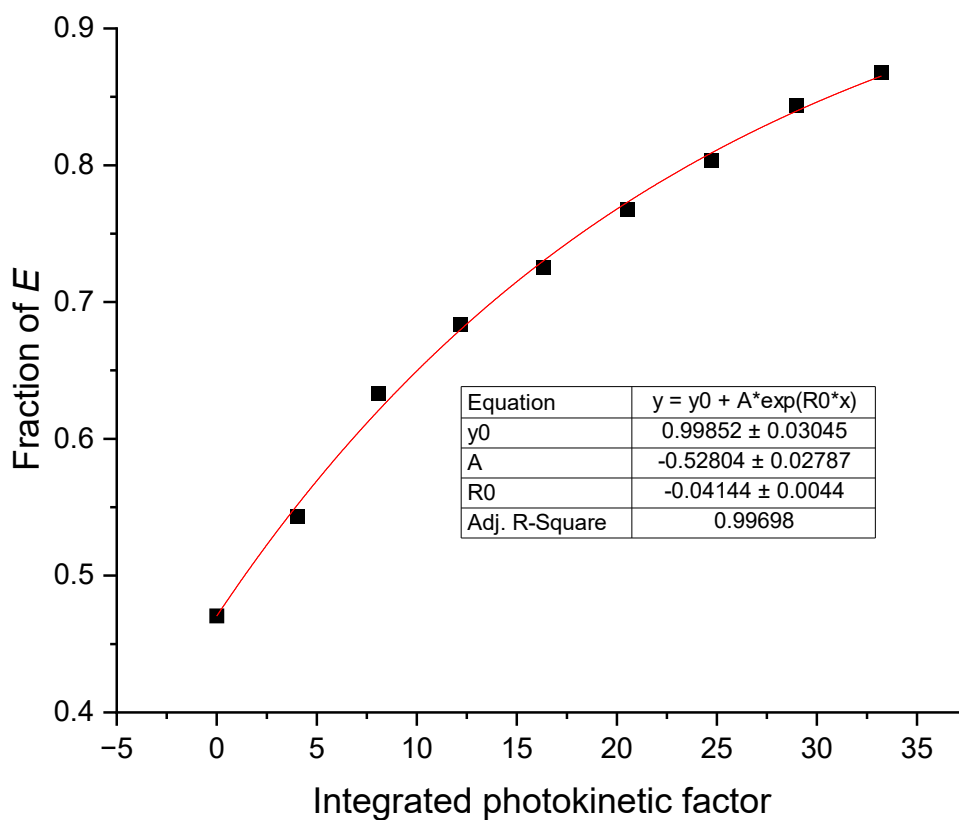


Figure S31. Exponential fitting of the *E* isomer fraction against integrated photokinetic factor $x(t)$. $\epsilon_{1-E@410 \text{ nm}} = 9,300 \text{ M}^{-1}\cdot\text{cm}^{-1}$ was used for quantum yield calculations. The photoisomerization quantum yield of **1-Z** to **1-E** in toluene ($1 \times 10^{-5} \text{ M}$) at 298 K was calculated to be $15.8 \pm 0.1 \%$ based on three consecutive measurements.

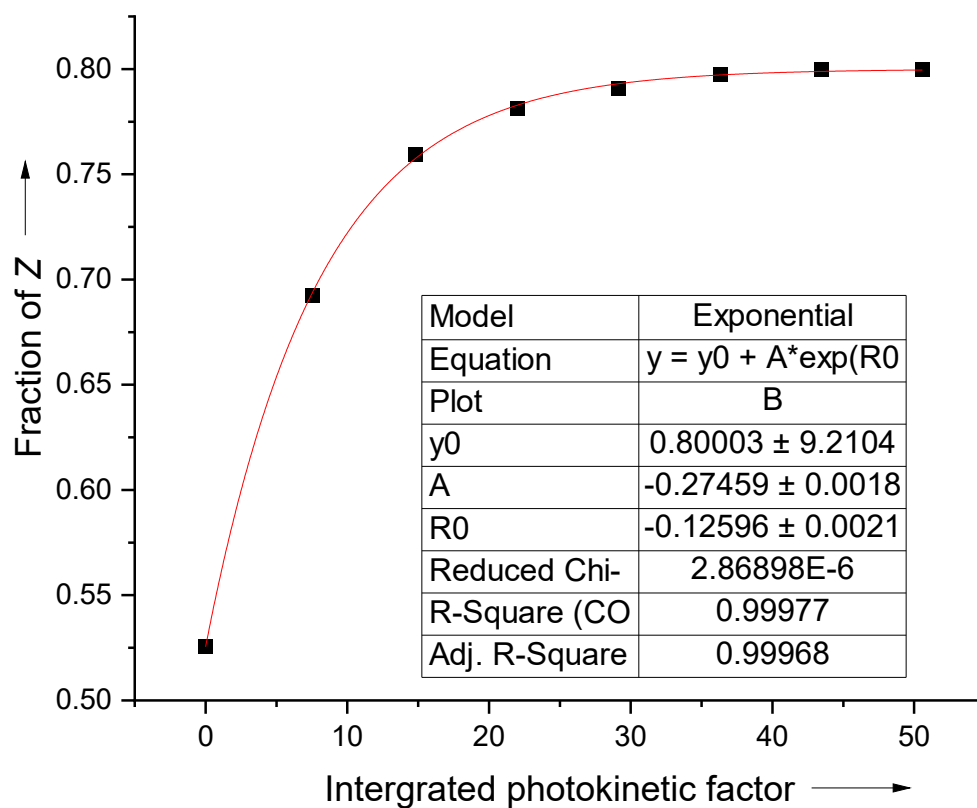


Figure S32. Exponential fitting of the *E* isomer fraction against integrated photokinetic factor $x(t)$. $\epsilon_{2-E@340 \text{ nm}} = 9,700 \text{ M}^{-1}\cdot\text{cm}^{-1}$ was used for quantum yield calculations. The photoisomerization quantum yield of **2-E** to **2-Z** in toluene ($1 \times 10^{-5} \text{ M}$) at 298 K was calculated to be $30.2 \pm 2.5 \%$ based on three consecutive measurements.

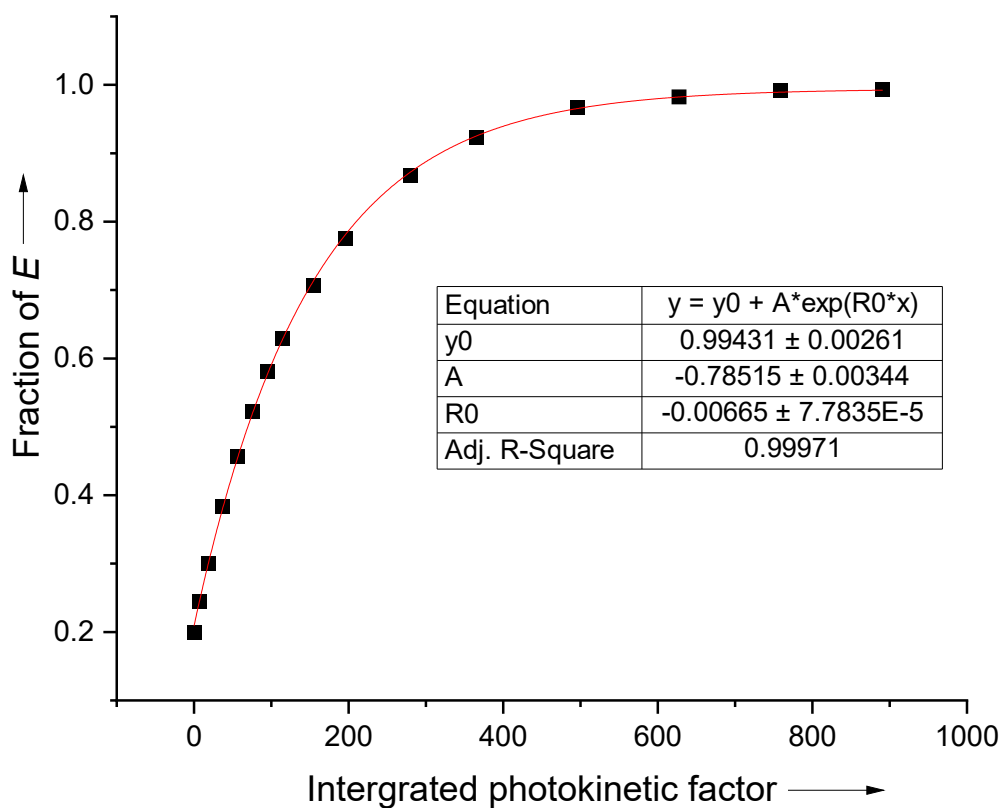


Figure S33. Exponential fitting of the *E* isomer fraction against integrated photokinetic factor $x(t)$. $\epsilon_{2-Z@442 \text{ nm}} = 700 \text{ M}^{-1} \cdot \text{cm}^{-1}$ was used for quantum yield calculations. The photoisomerization quantum yield of **2-Z** to **2-E** in toluene ($1 \times 10^{-5} \text{ M}$) at 298 K was calculated to be $51.7 \pm 0.4 \%$ based on three consecutive measurements.

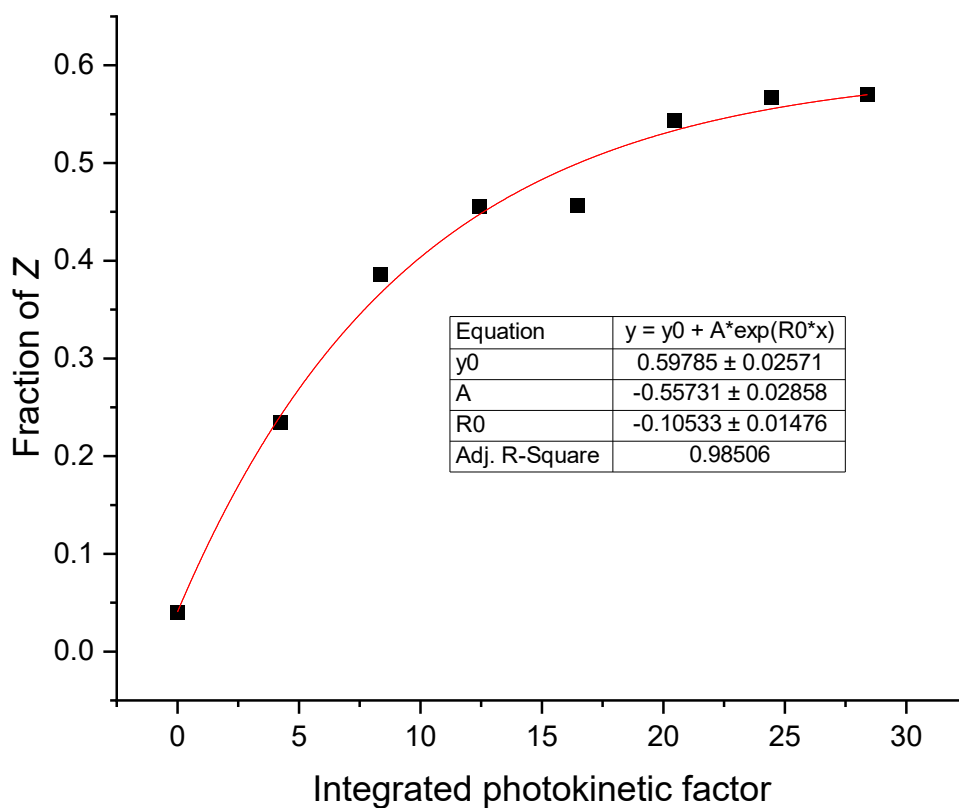


Figure S34. Exponential fitting of the *Z* isomer fraction against integrated photokinetic factor $x(t)$. $\epsilon_{3-E@340 \text{ nm}} = 10,300 \text{ M}^{-1} \cdot \text{cm}^{-1}$ was used for quantum yield calculations. The photoisomerization quantum yield of **3-E** to **3-Z** in toluene ($1 \times 10^{-5} \text{ M}$) at 298 K was calculated to be $15.3 \pm 0.6 \%$ based on three consecutive measurements.

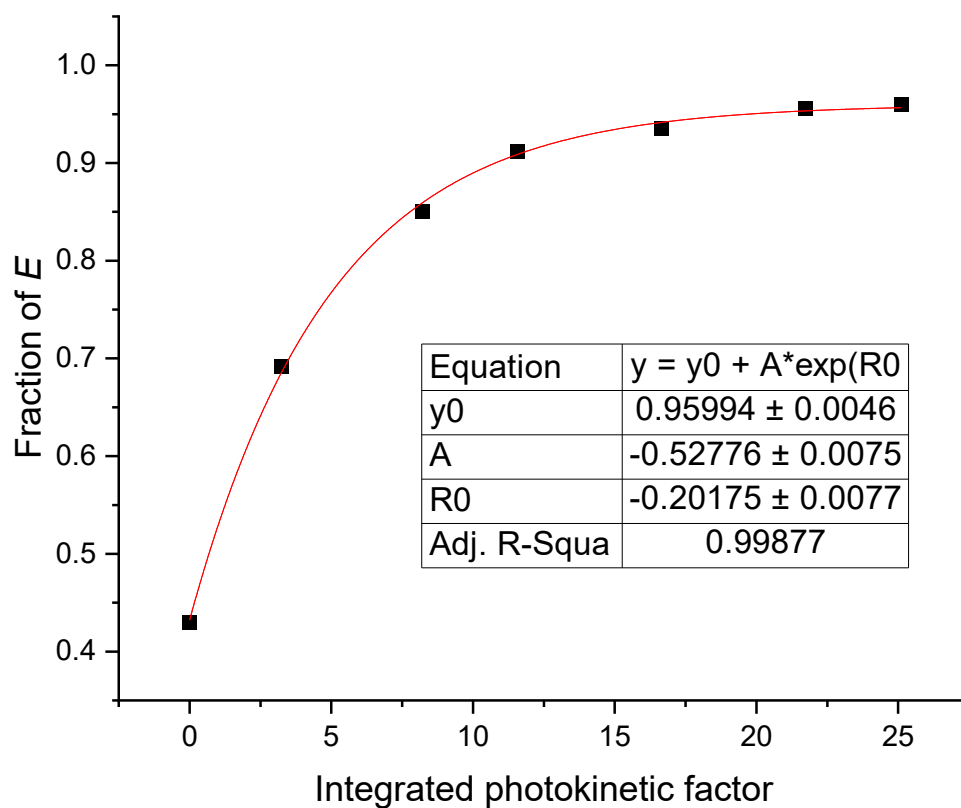


Figure S35. Exponential fitting of the *E* isomer fraction against integrated photokinetic factor $x(t)$. $\epsilon_{3-Z@442 \text{ nm}} = 16,100 \text{ M}^{-1} \cdot \text{cm}^{-1}$ was used for quantum yield calculations. The photoisomerization quantum yield of **3-Z** to **3-E** in toluene ($1 \times 10^{-5} \text{ M}$) at 298 K was calculated to be $44.9 \pm 3.3 \%$ based on three consecutive measurements.

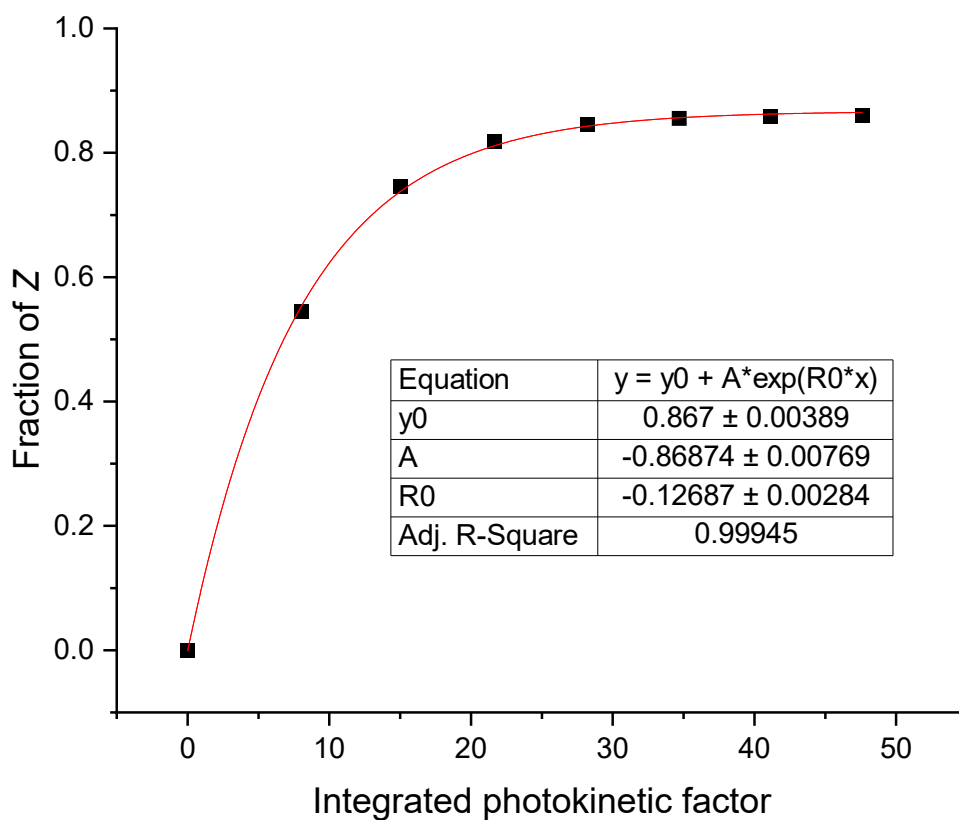


Figure S36. Exponential fitting of the Z isomer fraction against integrated photokinetic factor $x(t)$. $\epsilon_{4-E@340 \text{ nm}} = 15,500 \text{ M}^{-1} \cdot \text{cm}^{-1}$ was used for quantum yield calculations. The photoisomerization quantum yield of 4-E to 4-Z in toluene ($1 \times 10^{-5} \text{ M}$) at 298 K was calculated to be $17.9 \pm 0.4 \%$ based on three consecutive measurements.

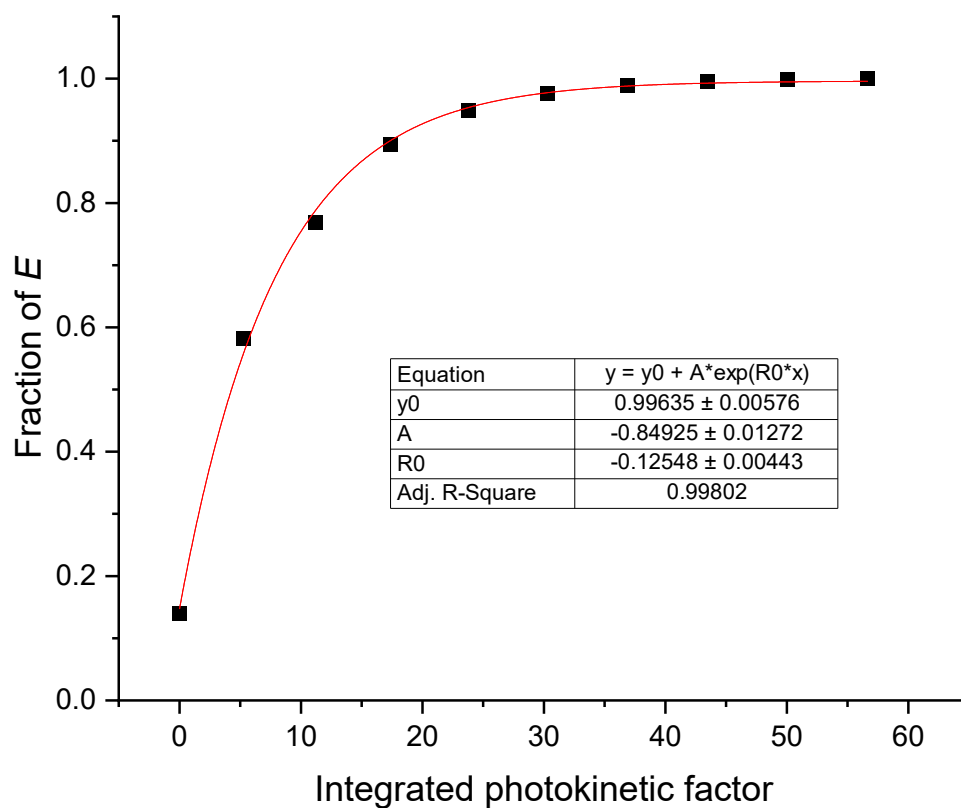


Figure S37. Exponential fitting of the *E* isomer fraction against integrated photokinetic factor $x(t)$. $\epsilon_{4-Z@442 \text{ nm}} = 10,200 \text{ M}^{-1}\cdot\text{cm}^{-1}$ was used for quantum yield calculations. The photoisomerization quantum yield of **4-Z** to **4-E** in toluene ($1 \times 10^{-5} \text{ M}$) at 298 K was calculated to be $47.5 \pm 0.7 \%$ based on three consecutive measurements.

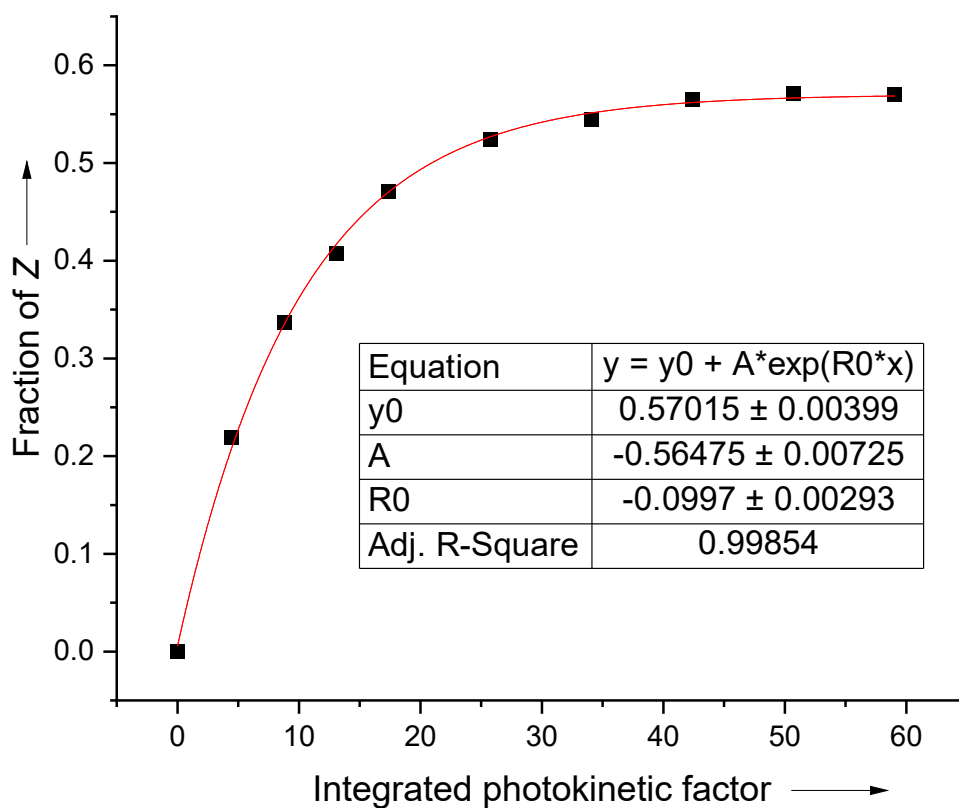


Figure S38. Exponential fitting of the Z isomer fraction against integrated photokinetic factor $x(t)$. $\epsilon_{5-E@340 \text{ nm}} = 12000 \text{ M}^{-1} \cdot \text{cm}^{-1}$ was used for quantum yield calculations. The photoisomerization quantum yield of **5-E** to **5-Z** in toluene ($1 \times 10^{-5} \text{ M}$) at 298 K was calculated to be $11.8 \pm 0.6 \%$ based on three consecutive measurements.

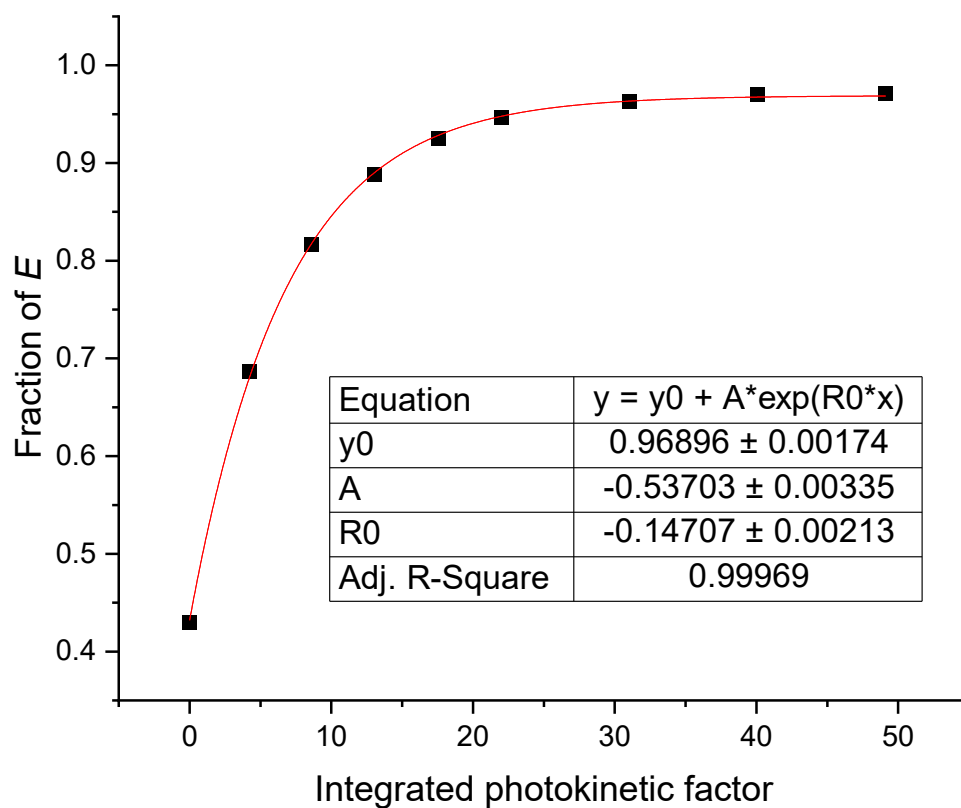


Figure S39. Exponential fitting of the *E* isomer fraction against integrated photokinetic factor $x(t)$. $\epsilon_{5-Z@442 \text{ nm}} = 16500 \text{ M}^{-1} \cdot \text{cm}^{-1}$ was used for quantum yield calculations. The photoisomerization quantum yield of **5-Z** to **5-E** in toluene ($1 \times 10^{-5} \text{ M}$) at 298 K was calculated to be $34.2 \pm 0.8 \%$ based on three consecutive measurements.

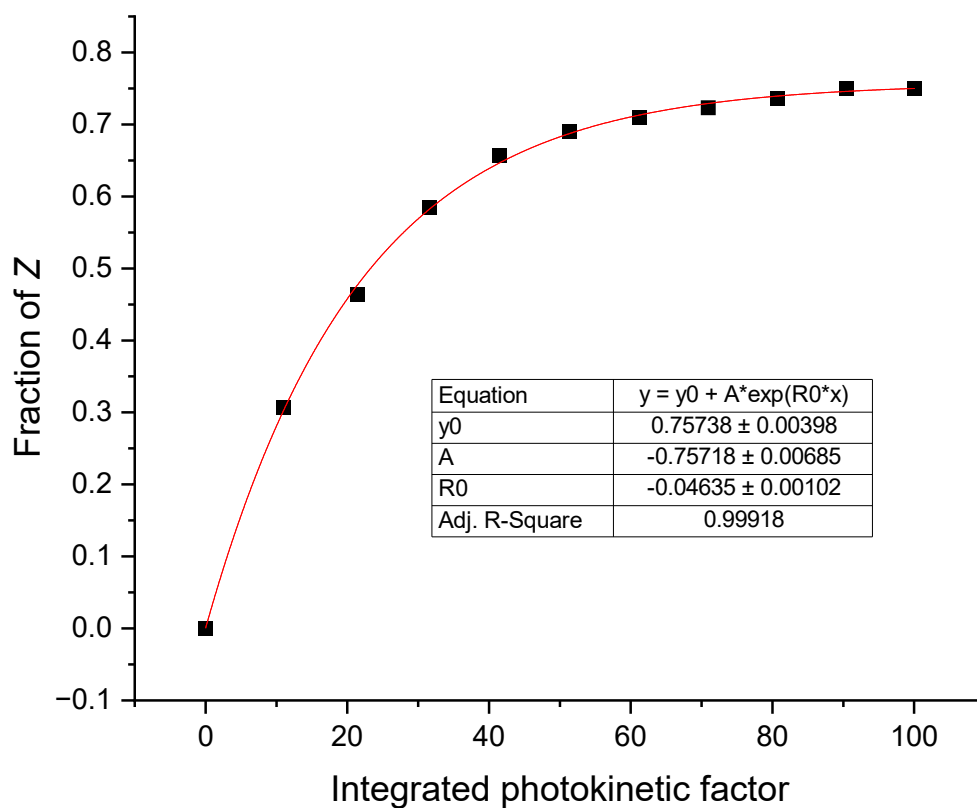


Figure S40. Exponential fitting of the *Z* isomer fraction against integrated photokinetic factor $x(t)$. $\epsilon_{6-E@340 \text{ nm}} = 13000 \text{ M}^{-1}\cdot\text{cm}^{-1}$ was used for quantum yield calculations. The photoisomerization quantum yield of **6-E** to **6-Z** in toluene ($1 \times 10^{-5} \text{ M}$) at 298 K was calculated to be $7.2 \pm 0.2 \%$ based on three consecutive measurements.

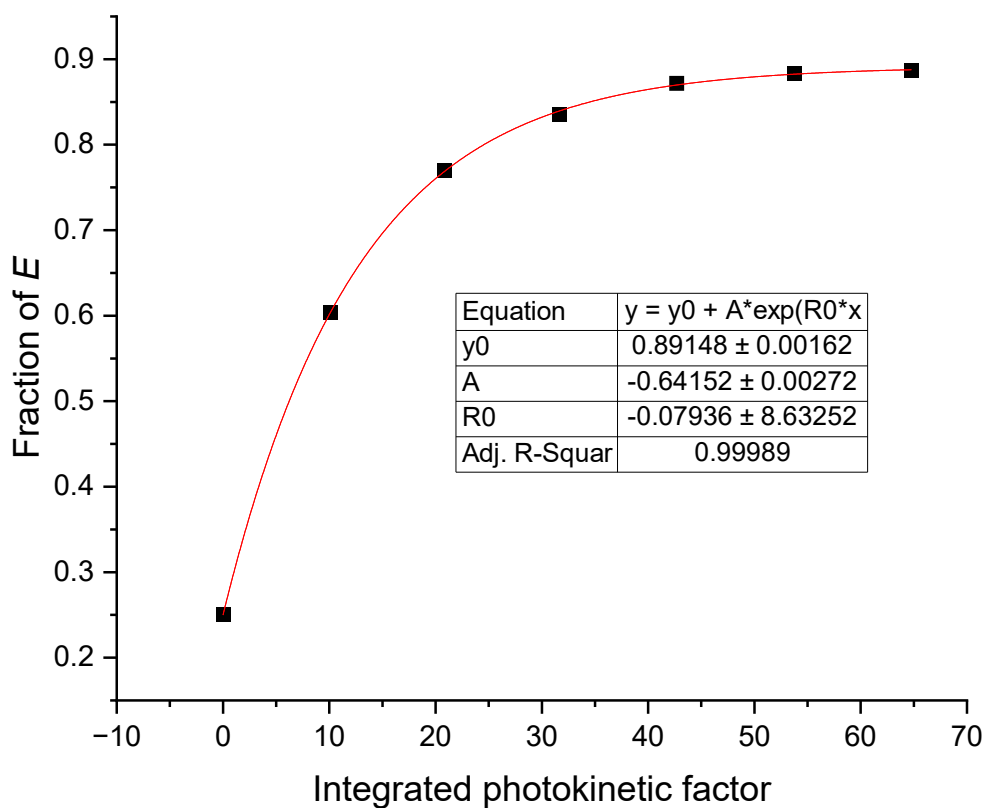


Figure S41. Exponential fitting of the *E* isomer fraction against integrated photokinetic factor $x(t)$. $\epsilon_{6-Z@480 \text{ nm}} = 12600 \text{ M}^{-1} \cdot \text{cm}^{-1}$ was used for quantum yield calculations. The photoisomerization quantum yield of **6-Z** to **6-E** in toluene ($1 \times 10^{-5} \text{ M}$) at 298 K was calculated to be $30.1 \pm 0.3 \%$ based on three consecutive measurements.

7. Raman Scattering Spectroscopy Studies

For the UV-Vis studies, a 1×10^{-3} M solution (3 mL) of the compound in spectroscopic grade toluene was loaded into a 1 cm quartz cuvette, and the spectra measured after reaching the appropriate PSS. Appropriate accumulation and acquisition times were selected for each hydrazone. The intensity of each spectrum was normalized to 1.

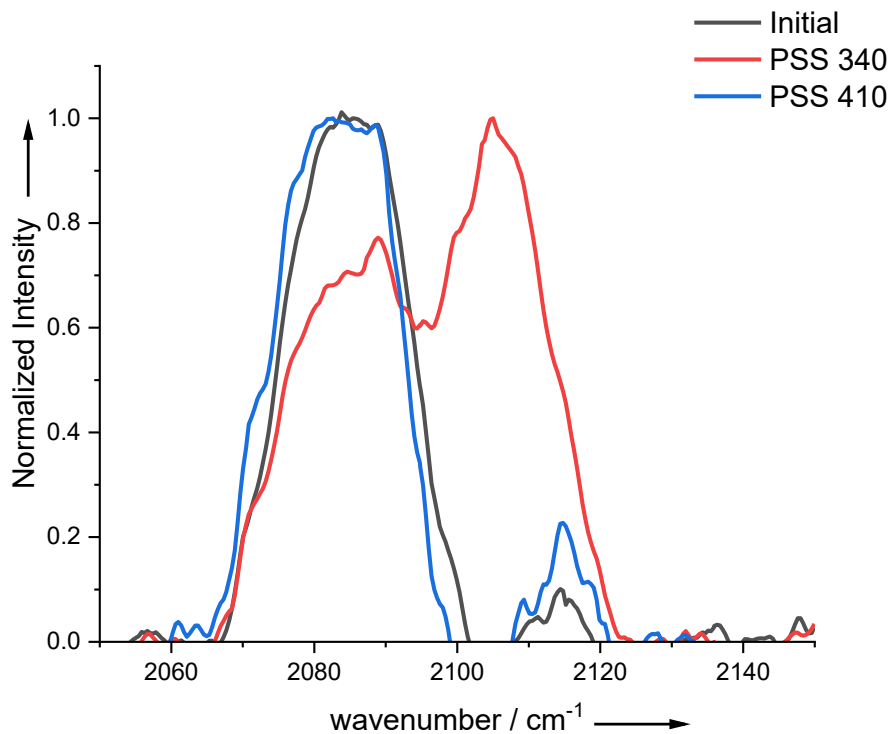


Figure S42. Raman spectra of **1** following light induced *Z/E* isomerization in toluene (1×10^{-3} M) at 298 K.

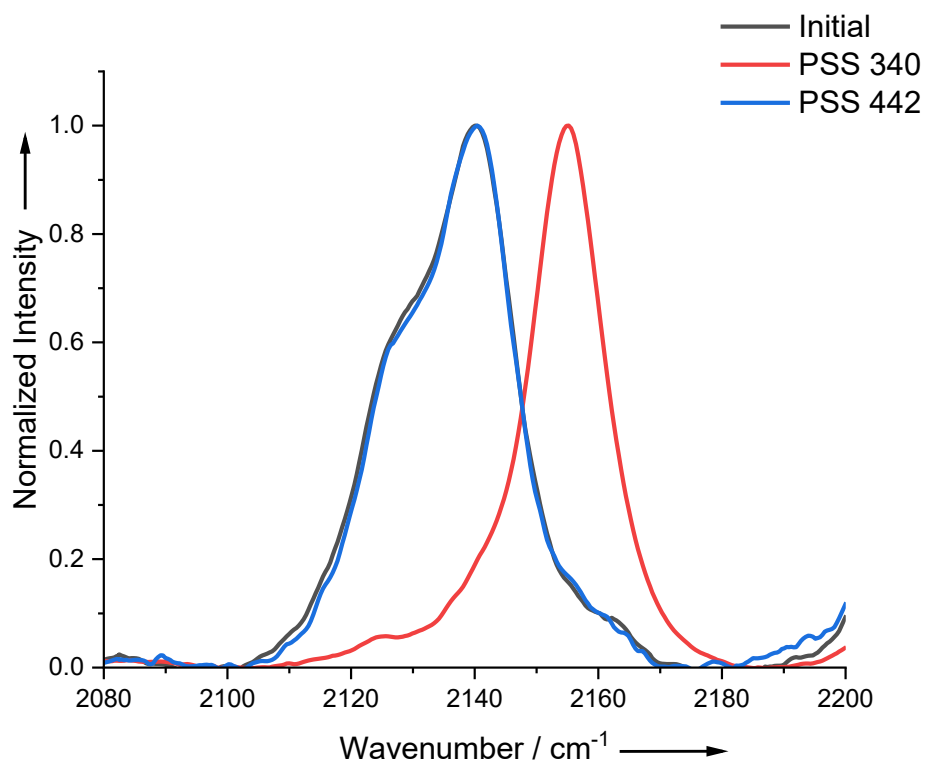


Figure S43. Raman spectra of **2** following light induced *Z/E* isomerization in toluene (1×10^{-3} M) at 298 K.

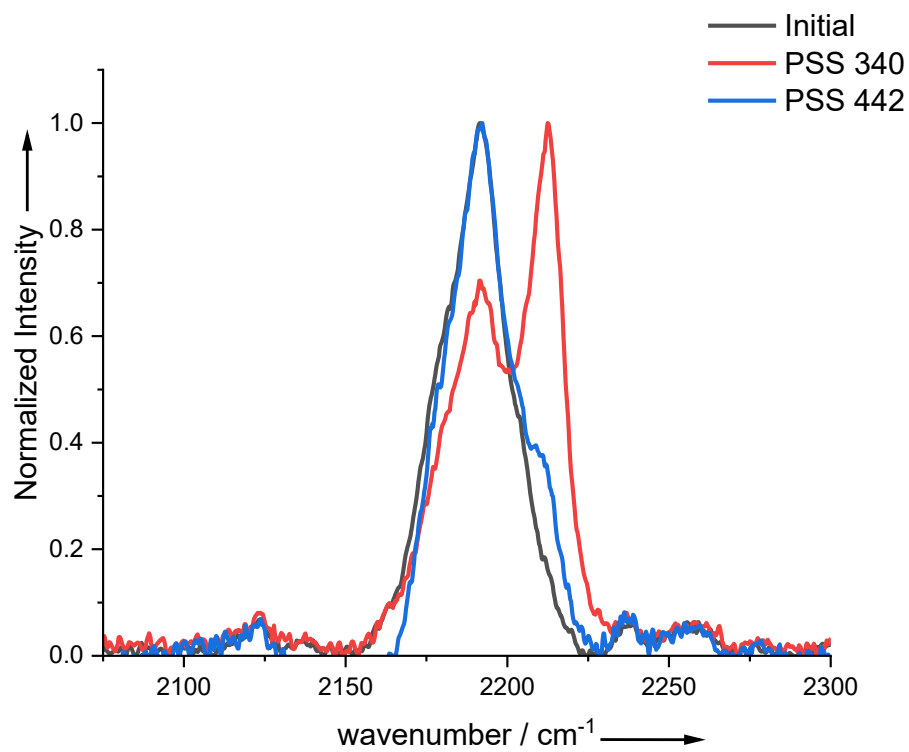


Figure S45. Raman spectra of **3** following light induced *Z/E* isomerization in toluene (1×10^{-3} M) at 298 K.

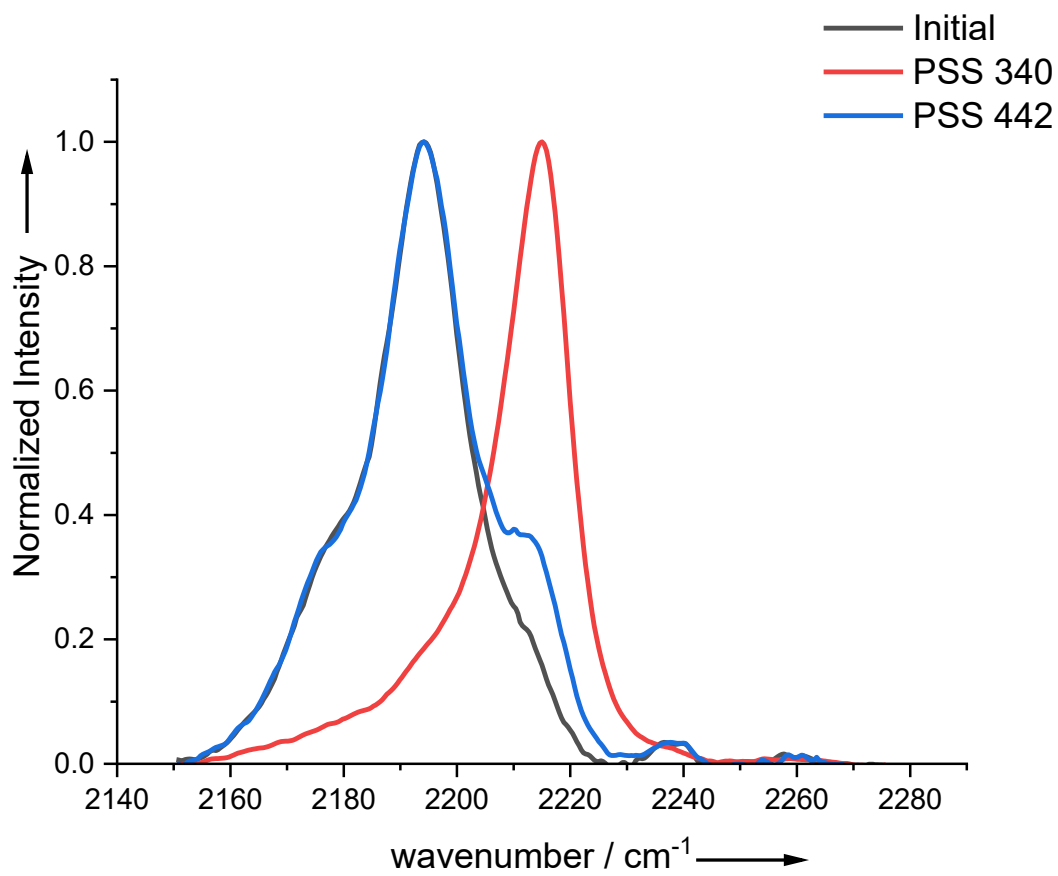


Figure S46. Raman spectra of **4** following light induced *Z/E* isomerization in toluene (1×10^{-3} M) at 298 K.

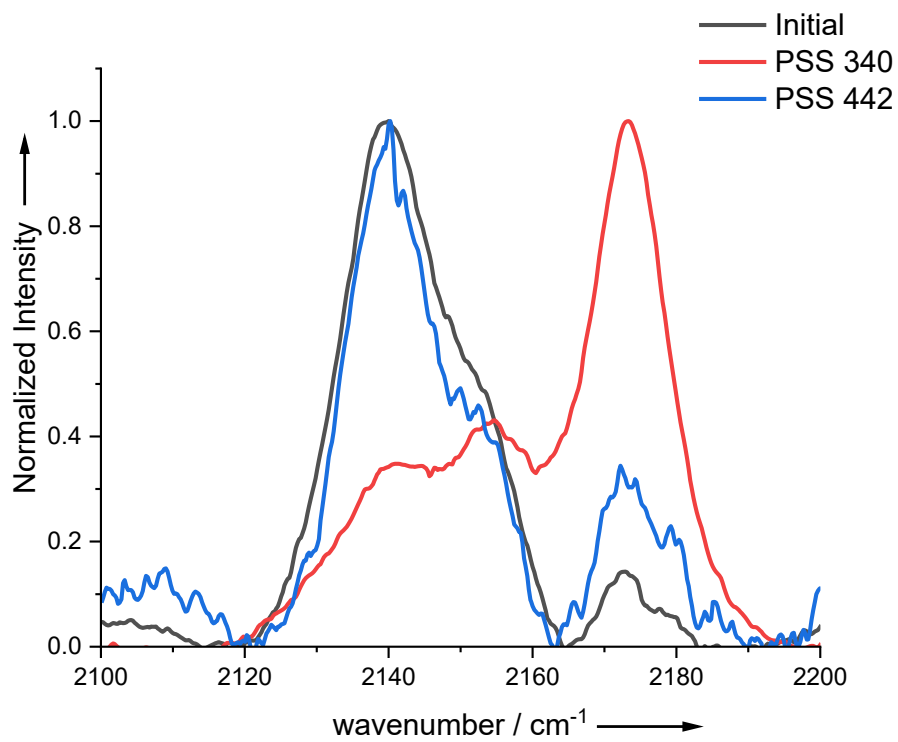


Figure S47. Raman spectra of **5** following light induced *Z/E* isomerization in toluene (1×10^{-3} M) at 298 K.

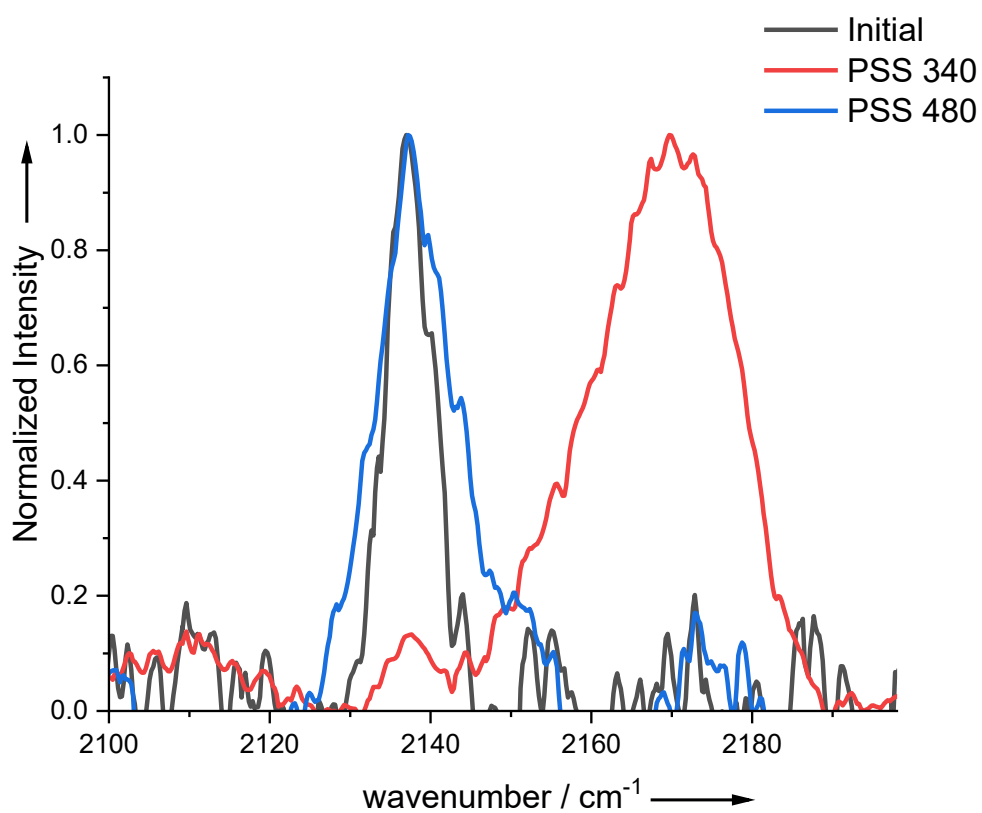
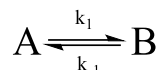


Figure S48. Raman spectra of **6** following light induced *Z/E* isomerization in toluene (1×10^{-3} M) at 298 K.

8. Kinetic Studies

The thermal half-lives of hydrazones **1-6** were estimated by following a reported procedure.^{S5} A solution of the appropriate hydrazone (1×10^{-3} M) in toluene-*d*₈ was prepared and then irradiated at 340 nm to obtain a *Z* rich solution, which was then heated at 90 °C under dark. The change in concentration of the *Z* isomer as a function of time was monitored using ¹H NMR spectroscopy. The thermal isomerization rates (k_1) were determined by least-square curve fittings using an integrated and combined rate equation (Eq. 8) of a single species reversible reaction.



$$K_{eq} = \frac{k_1}{k_{-1}} = \frac{C_A^0 - C_A^{eq}}{C_A^{eq}} \quad \text{Eq. 6}$$

$$\ln \frac{C_A - C_A^{eq}}{C_A^0 - C_A^{eq}} = -(k_1 + k_{-1})t \quad \text{Eq. 7}$$

Combining Eq. 6 and 7 will give Eq. 8 as follows,

$$C_A = (C_A^0 - C_A^{eq}) \times e^{\left(\frac{-k_1 \cdot C_A^0 \cdot t}{C_A^0 - C_A^{eq}}\right)} + C_A^{eq} \quad \text{Eq. 8}$$

where C_A , C_A^0 , and C_A^{eq} stand for experimental, initial, and equilibrium concentrations of the metastable configuration of the hydrazone switch, respectively; t stands for the thermal relaxation time.

Typical fits are shown in Figures S40-S44. The resulting k_1 values at 363 K were then used to calculate the energy barriers for the $E \rightarrow Z$ thermal relaxation using the Eyring equation (Eq. 9.) With the energy barriers (ΔG^\ddagger) in hand, the Arrhenius equation (Eq. 10) was used to extrapolate the rate constants (k_2) at 298K, from which the room-temperature thermal half-lives were determined

$$\Delta G^\ddagger = 8.314 \cdot T \cdot [23.760 + \ln \left(\frac{T}{k}\right)] \quad \text{Eq. 9}$$

where ΔG^\ddagger indicates the energy barrier to relaxation in J mol⁻¹ and T is the incubation temperature.

$$\ln \frac{k_2}{k_1} = \frac{\Delta G}{R} \left(\frac{1}{T_1} - \frac{1}{T_2}\right) \quad \text{Eq. 10}$$

where k_2 indicates the rate at the room temperature, k_1 indicates the rate at the incubation

temperature, R indicates the ideal gas constant in $\text{J K}^{-1} \text{mol}^{-1}$, T_2 is 298 K, and T_1 indicates the incubation temperature in K.

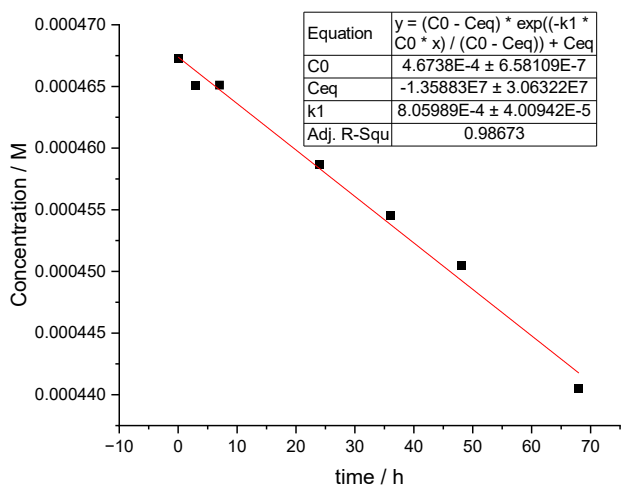


Figure S40. Thermal isomerization of **1-Z** \rightarrow **1-E** in toluene- d_8 at 363 K. The plot is of the concentration of **1-E** as a function of time. The resulting k_1 value was calculated to be $(1.2 \pm 0.1) \times 10^{-11} \text{ s}^{-1}$ based on three consecutive measurements at this temperature.

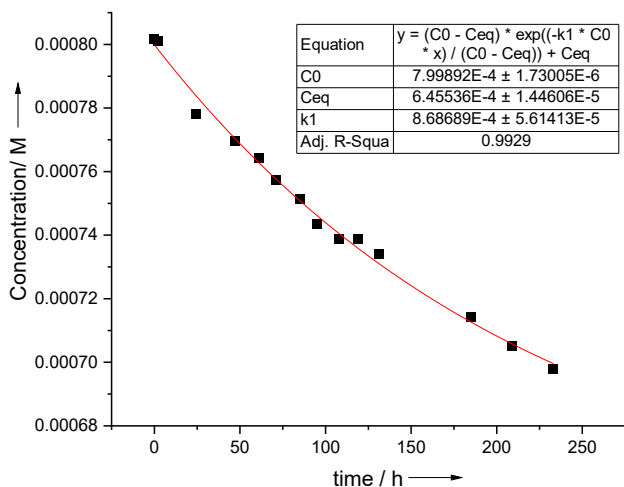


Figure S41. Thermal isomerization of **2-Z** \rightarrow **2-E** in toluene- d_8 at 363 K. The plot is of the concentration of **2-E** as a function of time. The resulting k_1 value was calculated to be $(8.0 \pm 0.8) \times 10^{-12} \text{ s}^{-1}$ based on three consecutive measurements at this temperature.

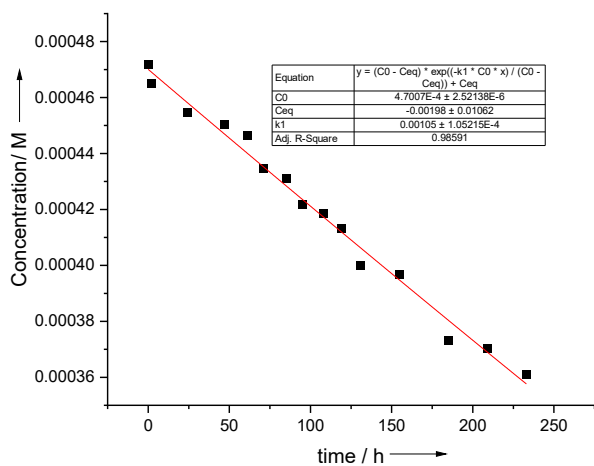


Figure S42. Thermal isomerization of **3-Z** \rightarrow **3-E** in toluene- d_8 at 363 K. The plot is of the concentration of **3-E** as a function of time. The resulting k_1 value was calculated to be $(1.1 \pm 0.1) \times 10^{-11} \text{ s}^{-1}$ based on three consecutive measurements at this temperature.

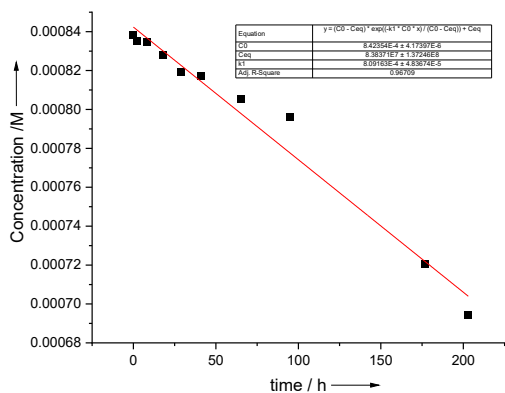


Figure S43. Thermal isomerization of **4-Z** \rightarrow **4-E** in toluene- d_8 at 363 K. The plot is of the concentration of **4-E** as a function of time. The resulting k_1 value was calculated to be $(8.3 \pm 0.5) \times 10^{-12} \text{ s}^{-1}$ based on three consecutive measurements at this temperature.

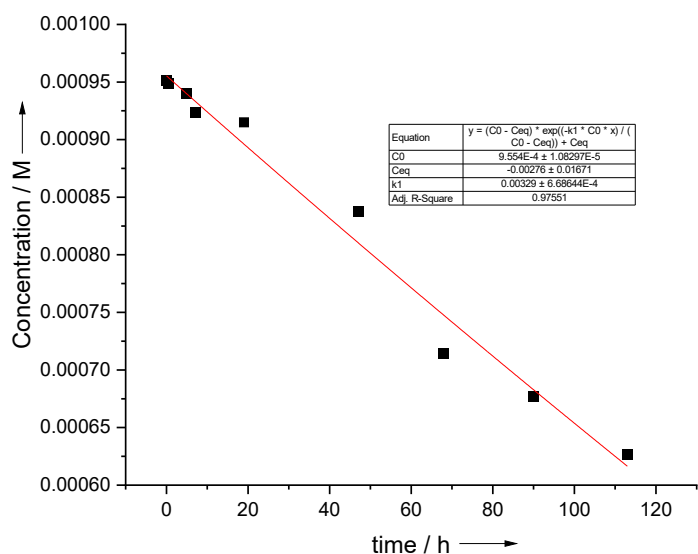


Figure S44. Thermal isomerization of **5-Z** \rightarrow **5-E** in toluene- d_8 at 366 K. The plot is of the concentration of **5-E** as a function of time. The resulting k_1 value was calculated to be $(4.2 \pm 0.1) \times 10^{-11} \text{ s}^{-1}$ based on three consecutive measurements at this temperature.

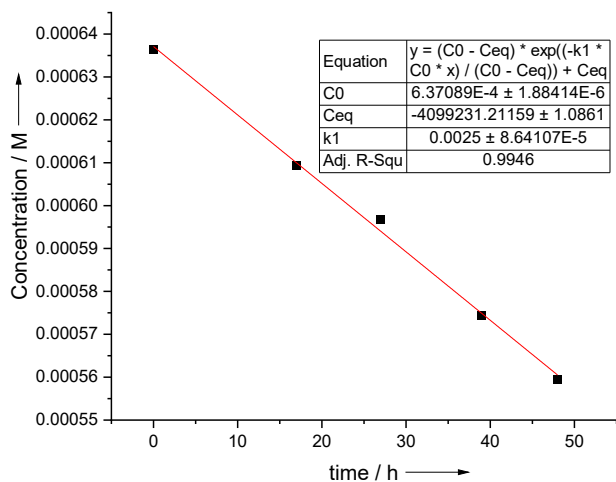


Figure S45. Thermal isomerization of **6-Z** \rightarrow **6-E** in toluene- d_8 at 363 K. The plot is of the concentration of **6-E** as a function of time. The resulting k_1 value was calculated to be $(6.4 \pm 0.4) \times 10^{-11} \text{ s}^{-1}$ based on three consecutive measurements at this temperature.

Table S1. The rate of the $Z \rightarrow E$ isomerization at 363 K, and energy barriers and half-lives extrapolated at 298 K.

Hydrazone	$k_{363\text{ K}} (\text{s}^{-1})^a$	$k_{298\text{ K}} (\text{s}^{-1})^a$	$\Delta G^\ddagger (\text{kcal mol}^{-1})^a$	$\tau_{1/2} (\text{years})$
1^b	$(2.2 \pm 0.1) \text{ E-07}$	$(1.2 \pm 0.1) \text{ E-11}$	32.4 ± 0.1	1710 ± 75
2^c	$(2.3 \pm 0.2) \text{ E-07}$	$(8.0 \pm 0.8) \text{ E-12}$	32.7 ± 0.1	2697 ± 235
3^c	$(2.9 \pm 0.1) \text{ E-07}$	$(1.1 \pm 0.1) \text{ E-11}$	32.5 ± 0.1	1929 ± 80
4^c	$(2.4 \pm 0.1) \text{ E-07}$	$(8.3 \pm 0.5) \text{ E-12}$	32.7 ± 0.1	2628 ± 123
5^c	$(8.8 \pm 0.1) \text{ E-07}$	$(4.2 \pm 0.1) \text{ E-11}$	31.7 ± 0.1	517 ± 13
6^b	$(8.3 \pm 0.5) \text{ E-07}$	$(6.1 \pm 0.4) \text{ E-11}$	31.5 ± 0.1	392 ± 45

- a.* Average of three measurements.
b. Measurements were made at 363 K.
c. Measurements were made at 366 K.

9. Single Crystal Diffraction Studies

Single crystals of compound **1** suitable for X-ray structural analysis were obtained by slow evaporation from acetonitrile solution at 258 K, while single crystals of **2-6** were obtained by slow evaporation from their DCM/hexane solutions at room temperature under dark. In general, an appropriate crystal was mounted on a nylon loop with paratone oil. Data were collected using a XtaLAB Synergy, Dualflex, HyPix diffractometer equipped with an Oxford Cryosystems low-temperature device. MSU Data were measured using ω scans using Cu K α radiation (micro-focus sealed X-ray tube, 50 kV, 1 mA). The total number of runs and images was based on the strategy calculation from the program CrysAlisPro 1.171.42.93a (Rigaku OD, 2023).^{S6} Cell parameters were retrieved using the CrysAlisPro 1.171.42.93a (Rigaku OD, 2023) software and refined using CrysAlisPro 1.171.42.93a (Rigaku OD, 2023). Data reduction was performed using the CrysAlisPro 1.171.42.93a (Rigaku OD, 2023) software which corrects for Lorentz polarization. The final completeness is 100.00 out to 80.273 in Q CrysAlisPro 1.171.42.93a (Rigaku Oxford Diffraction, 2023) Numerical absorption correction based on gaussian integration over a multifaceted crystal model Empirical absorption correction using spherical harmonics, implemented in SCALE3 ABSPACK scaling algorithm.

The structure was solved in the space group by using dual methods using the ShelXT (Sheldrick, 2015)^{S7} structure solution program. The structure was refined by Least Squares ShelXL incorporated in Olex2 software program. All non-hydrogen atoms were refined anisotropically. Hydrogen atom positions were calculated geometrically and refined using the riding model, except for the hydrogen atom on the non-carbon atom(s) which were found by difference Fourier methods and refined isotropically when data permits.

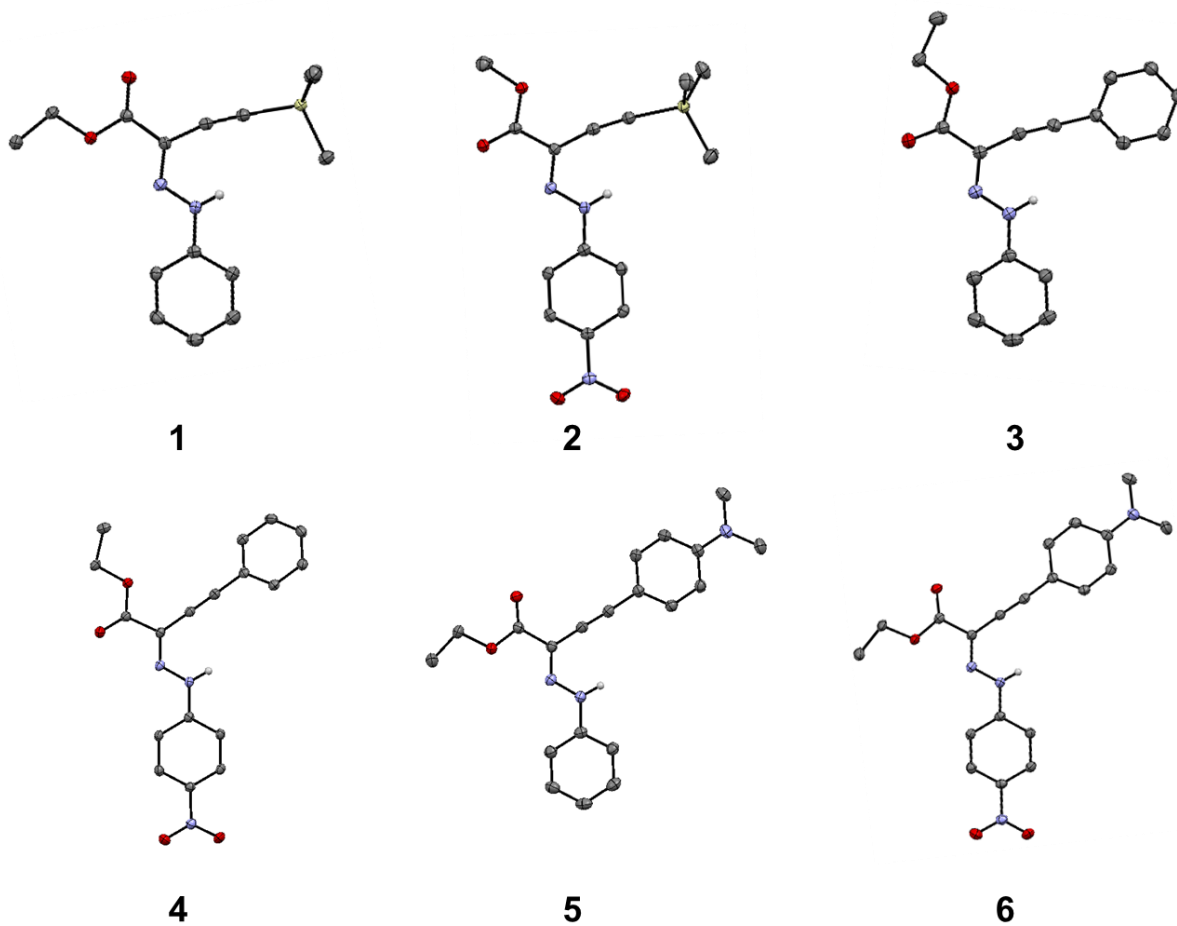


Figure S49. ORTEP drawing of the alkyne hydrazones **1-6** at the 50% probability level. The C-H hydrogens are omitted for clarity.

Table S2. Crystal Data and Parameters for Hydrazones 1 –4

	1	2	3	4
CCDC	2331026	2331028	2331030	2331032
Empirical formula	C ₁₅ H ₂₀ N ₂ O ₂ Si	C ₁₅ H ₁₉ N ₃ O ₄ Si	C ₁₈ H ₁₆ N ₂ O ₂	C ₂₀ H ₂₁ N ₃ O ₂
Formula weight	288.42	333.42	292.33	337.33
Temperature	100.00(10)	100.01(10)	99.99(10)	100.01(10)
Wavelength / Å	1.54184	1.54184	1.54184	1.54184
Crystal system	monoclinic	monoclinic	monoclinic	monoclinic
Space group	<i>P2₁/c</i>	<i>P2₁/c</i>	<i>I2/a</i>	<i>P2₁/c</i>
Unit cell dimensions	a = 6.9996(5) Å α = 90° b = 18.6210 (13)Å β = 90.611 (6) ° c = 12.0792(8)Å γ = 90°	a = 15.2895(10) Å α = 90° b = 10.2141(10) Å β = 93.648(10) ° c = 10.8354(10) Å γ = 90°	a = 13.2400(11) Å α = 90 ° b = 11.0359(11) Å β = 91.2541(7) ° c = 20.6586(17) Å γ = 90 °	a = 19.7442(3) Å α = 90° b = 6.9809(10) Å β = 93.3230(10)° c = 11.8207(2) Å γ = 90°
Volume / Å ³	1574.303(19)	1688.72(3) Å ³	3017.81(5) Å ³	1799.42(5) Å ³
Z	4	4	8	4
Z'	1	1	1	1
Density (Calcd.)	1.217	1.311	1.287	1.378
Absorption coefficient / mm ⁻¹	1.343	1.437	0.685	0.827
F(000)	616	704	1232	712
Crystal size / mm ³	0.27×0.22×0.13	0.40×0.18×0.07	0.20×0.16×0.11	0.24×0.19×0.03

θ range for data collection	4.363 to 80.273	2.896 to 80.360	4.281 to 80.299	2.241 to 80.339
Index ranges	$-8 \leq h \leq 8$	$-19 \leq h \leq 19$	$-16 \leq h \leq 16$	$-24 \leq h \leq 25$
	$0 \leq k \leq 23$	$0 \leq k \leq 12$	$0 \leq k \leq 13$	$-0 \leq k \leq 8$
	$0 \leq l \leq 15$	$0 \leq l \leq 13$	$0 \leq l \leq 26$	$-0 \leq l \leq 14$
Reflections measured	32803	18441	16466	16712
Independent reflections	3414 [Rint=0.0475]	3639 [Rint=0.0379]	3244 [Rint=0.0321]	3476 [Rint = 0.0317]
Data/restraints/parameters	/0/189	/0/216	/0/205	/0/231
Goodness-of-fit on F^2	1.032	1.056	1.076	1.053
Final R indexes [$I \geq 2\sigma(I)$]	$R_1 = 0.0329$, $\omega R_2 = 0.0874$	$R_1 = 0.355$, $\omega R_2 = 0.0958$	$R_1 = 0.0359$, $\omega R_2 = 0.0984$	$R_1 = 0.0394$, $\omega R_2 = 0.1089$
Final R indexes [all data]	$R_1 = 0.0337$, $\omega R_2 = 0.0881$	$R_1 = 0.376$, $\omega R_2 = 0.0980$	$R_1 = 0.0389$, $\omega R_2 = 0.1010$	$R_1 = 0.0439$, $\omega R_2 = 0.1136$
Largest diff. peak and hole	0.366 and -0.352 Å	0.346 and -0.312 Å	0.316 to -0.192 Å	0.341 to -0.293 Å

Table S3. Crystal Data and Parameters for Hydrazones 5 and 6

	5	6
CCDC	2421980	2421979
Empirical formula	C ₂₀ H ₂₁ N ₃ O ₂	C ₂₀ H ₂₀ N ₄ O ₄
Formula weight	335.40	380.40
Temperature	100.01(10)	100.01(10)
Wavelength / Å	1.54184	1.54184
Crystal system	triclinic	monoclinic
Space group	<i>P</i> -1	<i>I</i> 2/ <i>a</i>
Unit cell dimensions	a = 12.2715(18) Å α = 90.248(13)° b = 12.3986(18) Å β = 91.2744(13)° c = 12.5695 (2) Å γ = 109.7446(13)°	a = 12.6383(9) Å α = 90° b = 12.14363(11) Å β = 90.3855(8)° c = 24.6829(2) Å γ = 90°
Volume / Å ³	1799.42(5)	3788.11(6)
Z	4	8
Z'	2	1
Density (Calcd.)	1.238	1.334
Absorption coefficient / mm ⁻¹	0.653	0.785
F(000)	712	1600
Crystal size / mm ³	0.22×0.21×0.17	0.20×0.12×0.11
θ range for data collection	3.517 to 80.313	3.581 to 80.387
Index ranges	-15 ≤ h ≤ 15 -15 ≤ k ≤ 15 -16 ≤ l ≤ 0	-16 ≤ h ≤ 15 0 ≤ k ≤ 15 0 ≤ l ≤ 31

Reflections measured	38381	19891
Independent reflections	7712 [Rint = 0.0332]	4006
Data/restraints/parameters	/0/465	/0/261
Goodness-of-fit on F2	1.075	1.057
Final R indexes [$I \geq 2\sigma(I)$]	$R_1 = 0.0383$, $\omega R_2 = 0.1053$	$R_1 = 0.0345$, $\omega R_2 = 0.0938$
Final R indexes [all data]	$R_1 = 0.0410$, $\omega R_2 = 0.1076$	$R_1 = 0.0369$, $\omega R_2 = 0.0959$
Largest diff. peak and hole	0.184 to -0.231 Å	0.273 to -0.209 Å

9. References

- S1. M. Guo, D. Li, Z. Zhang, *J. Org. Chem.* 2003, **68**, 10172–10174
- S2. A. Sharma, P. Jamwal, H. Vaid, R. Gurubrahamam, *Org. Lett.* 2023, **25**, 1889–1894
- S3. D. Sosnin, M. Izadyar, S. A. A. Abedi, X. Liu, and I. Aprahamian, *J. Am. Chem. Soc.* 2025, xx, xxxx–xxxx
- S4. Y. He, Z. Shangguan, Z.-Y. Zhang, M, Xie, C, Yu, T. Li, *Angew. Chem., Int. Ed.* 2021, **60**, 16539–16546.
- S5. M. J. Moran, M. Magrini, D. M. Walba, I. Aprahamian., *J. Am. Chem. Soc.* 2018, **140**, 13623–13627
- S6. CrysAlisPro Software System, Rigaku Oxford Diffraction, (2023)
- S7. S. Khan, Q. N. Ahmed, *Eur. J. Org. Chem.*, 2016, **32**, 5377–5385